Bioactive Materials 25 (2023) 716–731

Contents lists available at ScienceDirect

Bioactive Materials

journal homepage: www.keaipublishing.com/en/journals/bioactive-materials

Silicate ions as soluble form of bioactive ceramics alleviate aortic aneurysm and dissection

Yumei Que [a,c,d], Zhaowenbin Zhang [b,e], Yanxin Zhang [c], Xin Li [c], Likai Chen [f], Peier Chen [g], Caiwen Ou [g], Chen Yang [a,c,d,*], Jiang Chang [a,b,c,d,e,**]

[a] Joint Centre of Translational Medicine, The First Affiliated Hospital of Wenzhou Medical University, Wenzhou, Zhejiang, 325000, China
[b] Shanghai Institute of Ceramics, Chinese Academy of Sciences (CAS), 1295 Dingxi Road, Shanghai, 200050, China
[c] Joint Centre of Translational Medicine, Wenzhou Institute, University of CAS, Wenzhou, Zhejiang, 325000, China
[d] Oujiang Laboratory, Wenzhou, Zhejiang, 325000, China
[e] Center of Materials Science and Optoelectronics Engineering, University of CAS, 19 Yuquan Road, Beijing, 100049, China
[f] Wenzhou Medical University, Wenzhou, Zhejiang, 325000, China
[g] Zhujiang Hospital, Southern Medical University, Guangzhou, Guangdong, 510280, China

ARTICLE INFO

Keywords:
Silicate ions
Aortic aneurysm and dissection
Senescence
Inflammation
Cell apoptosis

ABSTRACT

Aortic aneurysm and dissection (AAD) are leading causes of death in the elderly. Recent studies have demonstrated that silicate ions can manipulate multiple cells, especially vascular-related cells. We demonstrated in this study that silicate ions as soluble form of bioactive ceramics effectively alleviated aortic aneurysm and dissection in both Ang II and β-BAPN induced AAD models. Different from the single targeting therapeutic drug approaches, the bioactive ceramic derived approach attributes to the effect of bioactive silicate ions on the inhibition of the AAD progression through regulating the local vascular microenvironment of aorta systematically in a multi-functional way. The *in vitro* experiments revealed that silicate ions did not only alleviate senescence and inflammation of the mouse aortic endothelial cells, enhance M2 polarization of mouse bone marrow-derived macrophages, and reduce apoptosis of mouse aortic smooth muscle cells, but also regulate their interactions. The *in vivo* studies further confirm that silicate ions could effectively alleviate senescence, inflammation, and cell apoptosis of aortas, accomplished with reduced aortic dilation, collagen deposition, and elastin laminae degradation. This bioactive ceramic derived therapy provides a potential new treatment strategy in attenuating AAD progression.

1. Introduction

The world's population is aging rapidly. According to the most recent World Population Prospects (2019) from United Nations, the population over the age of 65 years has been more than 727 million (~9.3% of the world population) and will increase to over 1.54 billion (~15.9% of the world population) in 2050 [1]. In this age group, cardiovascular diseases (CVDs) result in 40% of all deaths since age constitutes the crucial risk factor for the development of CVDs [2]. Taking aortic aneurysm and dissection (AAD) diseases as an example, more than 4% of men over the age of 65 years are affected by AAD, which accounts for over 1% of deaths [3]. Although surgical treatments can significantly prevent aortic rupture and have saved thousands of AAD patients, the early mortality rate of post-surgical patients remains high (~9–25%), and the small asymptomatic AADs (<55 mm diameter in men and <50 mm diameter in women) are not recommended for surgery [4,5]. Further, serious post-surgical complications such as stroke, spinal cord infarction, and myocardial infarction may occur, which bring huge physical, mental, and economic burdens to the patients [6,7]. Therefore, it is urgent to develop new therapies for AAD treatment.

AADs are pathologically related to the endothelial dysfunction and degradation of the medial layer of aortic walls [8], which are more likely to appear in elderly people due to vascular senescence [9]. A typical AAD process is initiated by the overproduction of cytokines/chemokines

Peer review under responsibility of KeAi Communications Co., Ltd.
* Corresponding author. Joint Centre of Translational Medicine, Wenzhou Institute, University of CAS, Wenzhou, Zhejiang, 325000, China.
** Corresponding author. Joint Centre of Translational Medicine, The First Affiliated Hospital of Wenzhou Medical University, Wenzhou, Zhejiang, 325000, China.
E-mail addresses: cryangchen@ucas.ac.cn (C. Yang), jchang@mail.sic.ac.cn (J. Chang).

https://doi.org/10.1016/j.bioactmat.2022.07.005
Received 24 March 2022; Received in revised form 21 June 2022; Accepted 5 July 2022
Available online 16 July 2022

triggered by aging endothelial cells (ECs), which induce redundant inflammatory cell (IC) infiltration, resulting in abnormal apoptosis of vascular smooth muscle cells (SMCs), and destruction of extracellular matrix (ECM) [10–12]. In addition, an abundance of macrophages also infiltrate into aortic tunica media induced by inflammatory SMCs when AAD occurred [13]. These events lead to progressive dilation of the aortic wall, resulting in the formation of AAD and ultimately lethal aortic rupture. Therefore, regulation of vascular associated cells, especially from the aspects of alleviating EC senescence, regulating ICs, and protecting SMCs from apoptosis, is the key to suppressing the initiation and progression of AAD.

Currently, several drug therapies have been reported to restrict AAD progression through the regulation of transforming growth factor-beta (TGF-β) [14] or renin-angiotensin system (RAS) signaling pathways [15–17]. For example, statins are found to depress AAD formation by reducing the secretion of pro-inflammatory proteins, including matrix metalloproteinase (MMP)-9, monocyte chemoattractant protein (MCP)-2, and epithelial neutrophil-activating peptide (CXCL5) through the inhibition of the Rac1/NF-κB pathway [18]. Angiotensin-converting enzyme (ACE) inhibitors are found to suppress AAD in mice by attenuating aortic wall connective tissue destruction due to the inhibition of RAS activation [19,20]. Unfortunately, none of these medications, including statins and ACE inhibitors have been proved to efficiently attenuate AAD growth or rupture in the clinic after adjusting for other risk factors such as smoking and hypertension [16,21]. Since AAD progression is a multi-stage process including EC senescence, inflammation and SMC apoptosis, therapies targeting one stage of the processes may not be effective enough for AAD treatment. In our previous studies of biomaterials for regenerative medicine, we found that the silicate ions derived from bioactive calcium silicate bioceramics play a significant role in regulating microenvironment related to damaged tissues/organs, which contributes to the tissue/organ regeneration by provoking cellular activities of multiple cells including the stimulation of EC proliferation and angiogenesis [22,23], as well as the regulation of macrophage polarization and cell apoptosis [24,25]. These findings suggest that silicate ions derived from $CaSiO_3$ bioceramics might be able to regulate cells involved in three main stages of the AAD progression simultaneously including the regulation of ECs, macrophages, SMCs, and their interaction in the AAD progression more effectively.

To verify our hypothesis, we studied the effects of silicate ions derived from $CaSiO_3$ bioceramics on EC senescence, macrophage polarization, SMC apoptosis as well as the interaction between ECs (or SMCs) and ICs. Moreover, both angiotensin II (Ang II) and beta-aminopropionitrile (β-BAPN) induced AAD mouse models were established to verify the therapeutic effects of silicate ions derived from silicate bioceramics on reducing the mortality and AAD incidence rate, as well as reducing the aortic dilation, collagen deposition, elastin laminae degradation, senescence, inflammation, and cell apoptosis of aorta. Such a proof-of-concept study provides a new strategy for the development of AAD therapy.

2. Materials and methods

2.1. Preparation of silicate ions derived from $CaSiO_3$ bioceramics

According to ISO/EN 10993-12, the silicate ions extracts were prepared by soaking 1 g of calcium silicate ceramic powder (Kunshan Chinese Technology New Materials Co., LTD, Jiangsu, China) in 5 mL of serum-free high glucose Dulbecco's Modified Eagle Medium (DMEM) or saline and incubated at 37 °C for 24 h. The suspension was then centrifuged at 5000 rpm for 15 min and the supernatant was collected for sterilizing using a 0.22 μm filter (Millipore, USA). Silicate ions extracts diluted in DMEM with different dilution ratios (1/8, 1/16, 1/32, and 1/64) were prepared for cell experiments. Silicate ions extracts diluted in saline were prepared for animal experiments. An inductively coupled plasma mass spectrometer (ICP-MS, Agilent 7850, USA) was used to determine the concentrations of calcium and silicate ions in extracts.

2.2. Cell isolation and culture

The mouse bone marrow-derived macrophages (MBMMs) were isolated and differentiated using a standard protocol [26]. Briefly, primary MBMMs were isolated from 2-mouth-old mice and cultured in high glucose DMEM supplemented with 10% fetal bovine serum (FBS), 20% L929-conditioned medium, and 1% penicillin/streptomycin (P/S) for 6–7 days for differentiation. Both the primary mouse aortic endothelial cells (MAECs) and the primary mouse aortic smooth muscle cells (MASMCs) were purchased from Mingzhou Biotechnology Co., LTD (Zhejiang, China) and cultured in high glucose DMEM medium supplemented with 10% FBS and 1% P/S in a humid atmosphere of 5% CO_2 at 37 °C. Monocytes (Tohoku Hospital Pediatrics-1,THP-1) cell line was acquired from Cell Bank of Chinese Academy of Sciences and cultured in RPMI-1640 medium supplemented with 10% FBS and 1% P/S in a humid atmosphere of 5% CO_2 at 37 °C. The identity of MAECs and MASMCs was assessed by immunofluorescence staining of marker CD31 (Abcam, ab28364), and α-SMA (Abcam, ab7817), respectively. Both MAECs and MASMCs from passage 3 to 10 were used in this study. For lipopolysaccharide (LPS) induced inflammatory cell model, MAECs were seeded at a density of 2×10^4 cells/cm^2 in a six-well plate and cultured in high glucose DMEM supplemented with 10% FBS and 1% P/S for 12 h. Then, cells were cultured in LPS (10 μg mL^{-1}) containing media for 48 h and normal media for another 24 h in the absence/presence of silicate ions. Cells cultured in normal media for the whole time were used as control. For Angiotensin II (Ang II) induced cell apoptosis model, the MASMCs were seeded at a density of 2×10^4 cells/cm^2 in a six-well plate and cultured in high glucose DMEM supplemented with 10% FBS and 1% P/S for 12 h. Then, MASMCs were cultured in Ang II (10 μM L^{-1}) containing media for 48 h and normal media for another 24 h in the absence/presence of silicate ions. Cells cultured in normal media for the whole time were used as control.

2.3. Cell coculture

In MAECs (or MASMCs)-MBMMs direct contact coculture experiment, MAECs (or MASMCs) were seeded at a density of 2×10^4 cells/cm^2 in a six-well plate and cultured in high glucose DMEM supplemented with 10% FBS and 1% P/S for 12 h. Then, the medium was replaced by media with silicate ions, and cells were continuously cultured for 72 h. The silicate ion-free culture medium was used as a control. Subsequently, the MBMMs/monocytes (2×10^4/cm^2) were seeded on the cultured MAECs (or MASMCs) and incubated for 1 h. PBS was applied to rinse cells 3 times to remove the unbounded MBMMs/monocytes. 4–5 areas in each well were imaged and the number of bounded MBMMs was counted per image area. For LPS induced co-cultured cell model, MAECs were cultured in LPS (10 μg mL^{-1}) containing media for 48 h and normal media for another 24 h in the absence/presence of silicate ions. MAECs cultured in normal media for the whole time were used as control. Then, THP-1 (2×10^4/cm^2) cells were seeded on MAECs for 1 h and the number of bounded THP-1 cells was counted. In the MAECs-MBMMs indirect contact coculture experiment, the MAECs were seeded at a density of 2×10^4 cells/cm^2 in a six-well plate and cultured for 12 h. Then the culture medium was replaced by media with silicate ions for 72 h. Subsequently, the conditioned medium collected from MAECs was used to culture MBMMs for 48 h. Similarly, in the MBMMs-MASMCs indirect contact experiment, the isolated MBMMs were seeded at the density of 10^5 cells/cm^2 in a six-well plate and cultured for 6–7 days for differentiation, then the culture medium was replaced by the media with silicate ions for 72 h. The silicate ion-free culture medium was used as a control. The conditioned medium collected from MBMMs was further used to culture MASMCs for 48 h.

2.4. Cell counting kit-8 (CCK8) analysis

The MAECs and MASMCs were seeded on the 96-well plates at a density of 3×10^3 cells/cm^2 and cultured for 12 h in high glucose DMEM supplemented with 10% FBS and 1% P/S. Subsequently, the culture medium was replaced by media with silicate ions in different concentrations (diluted as 1/2, 1/8, 1/32, and 1/128), and cultured for 72 h. The silicate ion-free culture medium was used as a control. The cell viability was measured by a CCK8 assay kit (Dojindo, Kumamoto, Japan) according to the manufacturer's instructions. The absorbance was detected using a microplate reader (Synergy 2, BioTek, USA) at the wavelength of 450 nm.

2.5. Senescence-associated β-galactosidase (SA-β-gal) staining

The MAECs at passage 10 were seeded at a density of 2×10^4 cells/cm^2 in a six-well plate and cultured in high glucose DMEM supplemented with 10% FBS and 1% P/S for 12 h. Then, the medium was replaced by media with silicate ions, and cells were continuously cultured for 72 h. The silicate ion-free culture medium was used as a control. The pre-treated MAECs were washed with PBS 3 times followed by fixation with 4% paraformaldehyde (PFA). Then, SA-β-Gal staining assay was carried out using an SA-β-Gal staining kit (Beyotime, Shanghai, China) according to the manufacturer's instructions. The percentage of SA-β-Gal positive cells was estimated by counting at least 100 cells per replicate sample using the Image J software (National Institutes of Health, USA).

2.6. ELISA assay

Transforming growth factor-beta (TGF-β) was quantified using a mouse TGF-β ELISA kit (Dakewe Biotech Co., Ltd., Beijing, China) according to the manufacturer's instruction. Briefly, the conditioned medium collected from silicate ions treated MBMMs was diluted 10 times with PBS and added to a mouse TGF-β IgG coated 96-well plate and incubated for 1.5 h at room temperature. Then, the plate was rinsed 4 times with wash buffer provided in the kit and followed by the addition of the anti-mouse TGF-β antibody conjugated to horseradish. After 1 h incubation, the plate was washed 3 times with wash buffer and incubated for another 30 min with the substrate. The reaction was halted by the stopping buffer, and the optical density was recorded using a microplate reader (Synergy 2, BioTek, USA) at the wavelength of 450 nm. Data were calculated using the standard curve obtained from serial dilution of the standard substrate provided by the kit.

2.7. Protein isolation and Western blot analysis

Cells were lysed in cell lysis buffer (Beyotime Biotechnology, Shanghai, China). The obtained proteins were subjected to dodecyl sodium dodecyl sulfate-polyacrylamide gel electrophoresis (SDS-PAGE) and immunoblotted with specific antibodies against sirtuin-1 (Proteintech, 13161-1-AP), phospho-γH2A.X (Servicebio, GB111841), p65NF-κB (Proteintech, 10745-1-AF), Ac-NF-κB (Abbkine, ABP0029), VCAM1 (Santa Cruz, sc-13160), ICAM1 (Santa Cruz, sc-8439), caspase3 (Proteintech, 10380-1-AP), caspase9 (Proteintech, 19677-1-AP), or GAPDH (Abbkine, A01021). Proteins were visualized with an X-Ray film system (SUPER RX-N-C, Fujifilm, Japan) or a ChemiDoc™ XRS + System (Bio-Rad, USA). Densitometry analysis was performed using the Image J software (National Institutes of Health, USA), and the protein expression levels were normalized to GAPDH.

2.8. Flow cytometric analysis

For the analysis of MBMM polarization, PE anti-mouse F4/80 (BioLegend, 123109) and brilliant violet 650 anti-mouse CD206 (BioLegend, C068C2) antibodies were used. Briefly, more than 1×10^4 MBMMs were incubated with F4/80 antibody for 30 min at 4 °C and then treated with Cyto-Fast Fix/Perm (Biolegend, B335149) for cell membrane rupture. Subsequently, CD206 antibody was used to label MBMMs at 4 °C for 40 min. After the unbound antibodies were washed out, the labeled cells were analyzed using a BD FACS Celesta system (CytoFLEX, Beckman Coulter, USA). The percentage of M2 phenotype macrophages was defined as CD206$^+$ F4/80$^+$ cells gated from single cells. For the analysis of MASMCs apoptosis, an Annexin V-FITC Apoptosis Detection Kit (Beyotime, Shanghai, China) was used. Briefly, the silicate ions treated cells were re-suspended in apoptosis-positive control solution (195 μL) and then mixed with Annexin V-FITC (5 μL) and propidium iodide (PI, 10 μL), avoiding light for 20 min. The labeled cells were analyzed using a BD FACS Celesta system (CytoFLEX, Beckman Coulter, USA).

2.9. Murine AAD model and silicate ions treatment

Specific pathogen-free 49-day-old low-density lipoprotein receptor-deficient (LDLR$^{-/-}$) male mice in C57BL/6J background and 21-day-old male C57BL/6J mice were obtained from Gempharmatech Co., Ltd (Nanjing, China). The animal protocol and experimental procedures were approved by the Animal Research and Ethics Committee of Wenzhou Institute of University of Chinese Academy of Sciences (Approval Issue No. WIUCAS21061702 and WIUCAS20111901). For the Ang II-induced mouse model, experiments were performed according to the previously described protocol [27]. Briefly, 49-day-old LDLR$^{-/-}$ male mice were fed with a high-fat diet (HFD) and then subcutaneously implanted with ALZET osmotic pumps (Model 2004, DURECT Corporation, USA) containing Ang II (1.44 mg/kg/min, Calbiochem, 2787322) or PBS. After 7 days of Ang II or PBS infusion, 100 μL silicate ions contained saline or saline control was intravenously injected 7 times every other day. The experimental groups are defined as Ang II + Saline and Ang II + CS, respectively, while PBS + Saline was set as control. For beta-aminopropionitrile (β-BAPN)-induced mouse model, the experiment was performed according to the previously described protocol [28]. Briefly, 21-day-old male mice on a C57BL/6J background were fed with a regular diet and β-BAPN fumarate salt (0.8 g/kg/day, Sigma-Aldrich) containing water or free water for 4 weeks. After 7 days of β-BAPN administration, 100 μL silicate ions containing saline or saline control was intravenously injected 7 times every other day (Design I) or 14 times every day (Design II). The experimental groups are defined as β-BAPN + Saline β-BAPN + CS (Design I), and β-BAPN + H-CS (Design II), respectively, while H_2O + Saline was set as control. AAD analysis was performed after 28 days of Ang II or β-BAPN infusion and an autopsy was performed to determine the cause of death whenever the mouse dies. AAD is defined as a more than 50% increase in the maximal diameters of the suprarenal abdominal aorta or aortic arch by ultrasound imaging [29]. The whole aortas were isolated, and images were recorded with a stereomicroscope (SZ61TR, Nikon, Japan).

2.10. Blood pressure (BP) measurements

Arterial BP (systolic BP, diastolic BP and mean BP) was measured noninvasively on conscious mice by tail-cuff plethysmography (BP-2010A, Softron Biotechnology, Beijing, China) as previously described [30]. Briefly, each mouse was placed on a heating pad (37 °C) for 10 min to detect tail artery pulsations and pulse levels. Then, it was put in a plastic restrainer with its tail wrapped in a cuff containing a pneumatic pulse sensor. Before the official test, mice were trained for BP measurements every day for one week. Systolic BP, diastolic BP, and mean BP were measured at least five times and the averaged value was calculated, respectively.

2.11. Aortic ultrasonography monitoring

Ultrasound was performed with a high-resolution Vevo 2100 system (Visua Isonics, Toronto, Canada) equipped with a 30-MHz transducer

after mice were anesthetized. The maximal diameters of internal aortic arches or abdominal aortas were measured using the Vevo 2100 software (version 1.5.0). All recordings were made by a cardiologist or technician blinded to the experimental groups.

2.12. Histological analysis

Aortas were isolated, fixed with 4% PFA, embedded in optimal cutting temperature (OCT) compound (Sakura Finetek, USA) and stored at −80 °C. Seven-micrometer serial frozen sections were cut and stained with hematoxylin/eosin (HE) (Solarbio, G1120) for morphological analysis, Masson's trichrome (Solarbio, G1345) for collagen deposition, or modified Gomori (Solarbio, G1593) for elastin laminae degradation assessment. The collagen deposition was evaluated using a score of 1–4, where 1 = less than 25% area in medium layer was occupied by collagen, 2 = 25–50% collagen deposition, 3 = 50–75% collagen deposition, and 4 = > 75% collagen deposition. Elastin laminae degradation was evaluated by using a grade of I-IV as previously reported [13], where I = intact internal elastic lamina, II = mild elastin fragmentation, III = severe elastin digestion, and IV = severe elastin digestion with a visible ruptured site. The collagen deposition and elastin laminae degradation of aortic sections were quantified by 4 individual observers blinded to the experimental groups. The senescence of aortas was evaluated using SA-β-gal staining. Briefly, the fresh tissue section was fixed in 4% PFA for 10 min and then incubated with SA-β-gal working solution for 24 h at 37 °C followed by eosin counterstaining for 30 s. Images were captured and the percentage of SA-β-gal positive area versus total area was analyzed using the Image J software (National Institutes of Health, USA).

2.13. Immunohistochemistry and immunofluorescence staining

The obtained sections were heated for antigen retrieval in 10 mM citrate acid buffer before being blocked in goat serum. For immunochemistry, sections were incubated overnight at 4 °C with one of the following primary antibodies: rabbit anti-mouse VCAM1 (1:100), rabbit anti-mouse ICAM1 (1:100), rabbit anti-mouse caspase3 (1:200) or rabbit anti-mouse caspase9 (1:200). Then, the secondary antibody (biotinylated goat anti-rabbit IgG, Zsbio, pv-6001) was added and incubated at room temperature for 30 min. The immune complexes were visualized according to the staining procedure of the HRP-DAB kit (CWBIO, Beijing, China) and IgG acted as negative intensity control. The positive area (brown) was scored using a score of 0–4, where 0 = negative intensity, 1 = weak intensity, 2, 3 = medium intensity, and 4 = strong intensity as previously reported [31]. The staining of VCAM1, ICAM1, caspase3, and caspase9 were all quantified by 4 individual observers blinded to the experimental groups. For immunofluorescence, the sections or cells on glass coverslips were blocked with 5% BSA containing 0.1% Tween-20 for 60 min. Then the primary antibodies against F4/80 (Santa Cruz, sc-377009, 1:200) or γH2A.X (Servicebio, GB111841, 1:200) were incubated overnight at 4 °C followed by incubation with the secondary antibody of Cy3-conjugated Affinipure Goat Anti-Rabbit IgG (H + L) (Proteintech, SA00009-2, 1:400) or Fluorescein (FITC)-conjugated Affinipure Goat Anti-Mouse IgG (H + L) (Proteintech, SA00003-1, 1:400) for 120 min at room temperature. Cell nuclear was stained with 4′6-diamidino-2-phenylindole (DAPI, Solarbio, C0065) for 10 min. The fluorescence signals were monitored by a Nikon A1 confocal microscopy (Nikon, Japan) and analyzed by the NIS-Elements Viewer software (version 5.21.00). The percentage of γH2A.X positive cells was counted using the Image J software (National Institutes of Health, USA).

2.14. TUNEL staining

The TUNEL staining was applied using a TUNEL Apoptosis Assay kit (Beyotime, Shanghai, China). Briefly, sections of the aortas were fixed with 4% PFA for 10 min and then washed with PBS 3 times. The obtained sections were incubated with the TUNEL working solution provided in the kit at 37 °C for 2 h under dark conditions followed by the nuclear staining with DAPI. Fluorescence signals at 550 nm were monitored by a Nikon A1 confocal microscopy (Nikon, Japan) and analyzed by the NIS-Elements Viewer software (version 5.21.00). The mean fluorescence intensity of a cross-section was analyzed using the Image J software (National Institutes of Health, USA).

2.15. Toxicity evaluation

Heart, liver, spleen, lungs, and kidneys were isolated, fixed with 4% PFA for 12 h, and embedded with paraffin to prepare sections. Five-micrometer serial sections were cut and stained with HE (Solarbio, G1120) and images were captured for morphological analysis.

2.16. Statistical analysis

Data were presented as the mean ± SEM. Fold change over control was used in Western blot and fluorescence intensity analysis to avoid larger variation among different experiments. Statistical analysis was performed using the GraphPad Prism7 (Beijing, China). A two-sided unpaired Student's t-test was used to analyze data between the two groups. Nevertheless, differences were assessed by one-way analysis of variance (ANOVA) with Tukey's multiple comparison test for more than or equal 3 groups. Non-normally distributed data were analyzed by non-parametric analysis. $p < 0.05$ is considered statistically significant.

3. Results

3.1. Silicate ions derived from $CaSiO_3$ bioceramics alleviate senescence of the mouse aortic endothelial cells (MAECs)

Biomaterials can regulate the fate of vascular-related cells in different aspects including cell morphology, viability, proliferation, migration, and differentiation [32]. Our previous studies proved that silicate biomaterials could also manipulate cell behaviors including endothelial cell proliferation and migration [33,34]. Here, to investigate the effect of silicate ions derived from $CaSiO_3$ bioceramic on vascular-related cells, we first prepared silicate ion extracts with different dilution ratios similar to our previous studies [35,36]. The exact concentrations of silicate ions in the extracts with different dilution ratios were shown in Table S1. We found that the dilution ratios of 1/8, 1/32, and 1/128 significantly promoted the proliferation of both MAECs and the mouse aortic smooth muscle cells (MASMCs), especially for the dilution ratio of 1/8 (Fig. S1, A and B). Therefore, the silicate ion extract with the dilution ratio of 1/8 (silicate ion concentration: 11.72 ± 0.69 μg mL^{-1}) was chosen for the subsequent cell studies.

It is known that aging causes endothelial cell dysfunction and accelerates the formation of AAD [37,38]. To determine the role of silicate ions derived from $CaSiO_3$ bioceramics in inhibiting the senescence of MAECs, we treated the MAECs with silicate ions containing medium (CS) or control medium (Ctrl) for 72 h. A senescence-associated beta--galactosidase (SA-β-Gal) staining was firstly applied, and the results are shown in Fig. 1A. It is clear to see that the percentage of SA-β-Gal positive cells significantly decreased from 30.32 ± 2.24% to 20.82 ± 1.16% after the treatment with silicate ions. Then, we specifically analyzed the effect of silicate ions on the expression of the longevity regulator sirtuin-1 (SIRT1) in MAECs, which is an NAD^+-dependent deacetylase and normally downregulated in the aged aorta [39]. The Western blot (WB) assay showed that protein expression of SIRT1 was higher in the CS treated MAECs as compared to Ctrl (Fig. 1B). Moreover, the expression of DNA damage biomarker phosphorylated H2A.X (γH2A.X) was also evaluated by WB analysis, which was significantly reduced after the treatment of CS as compared to Ctrl (Fig. 1C). Since the nucleation of γH2A.X is closely correlated with aortic senescence [40], we further detected its nucleus expression using immunofluorescence staining. The

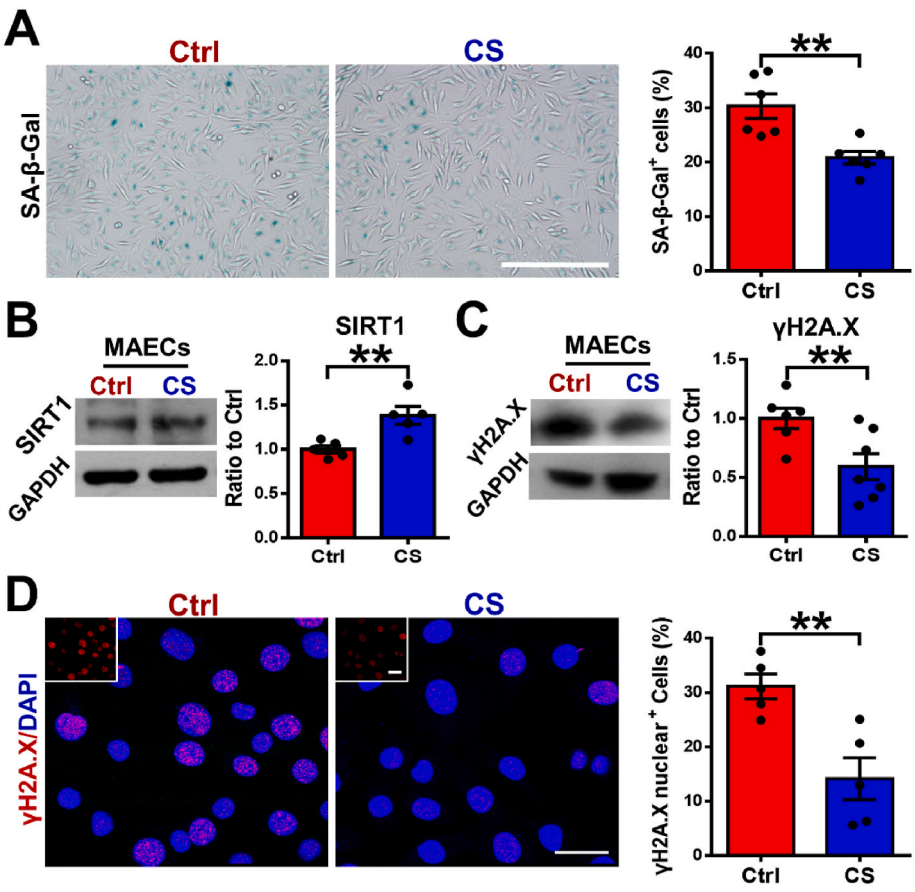

Fig. 1. Silicate ions as soluble form of bioactive ceramics alleviate senescence of MAECs. (A) SA-β-Gal (blue, senescence marker) staining and quantitative analysis of SA-β-Gal staining (presented as the percentage of SA-β-Gal positive cells) in cultured MAECs treated with Ctrl (n = 6) or CS (n = 6) for 72 h. (B) Representative Western blots of SIRT1 (senescence-associated protein) and quantitative analysis of protein levels presented as mean ratio values quantified from protein bands of SIRT1 versus GAPDH (an endogenous control for protein expression) in cultured MAECs treated with Ctrl (n = 5) or CS (n = 5) for 72 h. (C) Representative Western blots of γH2A.X (DNA damage-associated protein) and quantitative analysis of protein levels presented as mean ratio values quantified from protein bands of γH2A.X versus GAPDH in cultured MAECs treated with Ctrl (n = 6) or CS (n = 7) for 72 h. (D) Representative immunofluorescence images of γH2A.X (red)/DAPI (blue) and quantitative analysis of γH2A.X nuclear expression presented as the percentage of γH2A.X positive cells in cultured MAECs treated with Ctrl (n = 5) or CS (n = 5) for 72 h. The top left corner images show the γH2A.X staining of MAECs. Scale bars, 100 μm (A) and 50 μm (D). MAECs, mouse aorta endothelial cells. Ctrl, control medium. CS, silicate ions containing medium. All data are presented as mean ± SEM. Statistical analysis was performed using unpaired Student's t-test, **P < 0.01.

corresponding quantitative analysis confirmed that the expression of γH2A.X in CS treated MAECs was also significantly reduced since the percentage of γH2A.X positive cells decreased from 31.1 ± 2.26% to 14.14 ± 3.85% after the treatment of silicate ions (Fig. 1D). These observations implied that silicate ions derived from $CaSiO_3$ bioceramic may be protective against senescence of MAECs.

3.2. *Silicate ions derived from $CaSiO_3$ bioceramics alleviate MAECs inflammation and promote mouse bone marrow-derived macrophages (MBMMs) polarization*

The elevated expression of inflammatory cytokines, which are caused by senescent endothelial cells has been found to play a key role in vascular aging, leading to the initiation, progress, and advancement of cardiovascular disease [37]. Since nuclear factor kappa-B p65 (p65) is the core inflammatory transcription factor and its acetylation at lysine 310 (Ac-p65) is essential for the enhancement of the transcriptional activity [41], we firstly analyzed the effect of silicate ions on the expression of Ac-p65 in MAECs using WB assay. As shown in Fig. 2A, the expression of Ac-p65 was significantly reduced in MAECs after the treatment of silicate ions for 72 h. To confirm the anti-inflammatory effect of silicate ions on MAECs, we also evaluated the expression of the downstream effectors of p65 (vascular cell adhesion molecule 1 (VCAM1) and intercellular adhesion molecule 1 (ICAM1)) in MAECs with or without lipopolysaccharide (LPS, an inflammation mediator) treatment using WB assay. It is noted that without LPS treatment, the ICAM1 was significantly decreased in CS treated MAECs compared with Ctrl, although the expression of VCAM1 was comparable between those two groups (Fig. S2). After the LPS treatment, the expression of both ICAM1 of VCAM1 in MAECs was significantly increased (Fig. 2B). Interestingly, we found that the treatment of silicate ions only significantly down-regulated the expression of ICAM1, which was consistent with the result obtained in the cells without LPS treatment. Apart from MAECs, MBMMs also play a vital role in the inflammatory response during AAD progression and the induction of macrophage polarization to M2 phenotype is a commonly used anti-inflammatory strategy [42,43]. As shown in Fig. 2C, the percentage of M2 phenotype MBMMs was sharply increased from 5.92 ± 1.23% to 73.69 ± 6.82% after the treatment with silicate ions for 72 h, which was calculated using flow cytometric analysis with staining of phenotypic markers F4/80 (M0) and CD206 (M2). Moreover, the enhanced M2 phenotype polarization of CS treated MBMMs was further confirmed by ELISA assay of transforming growth factor-beta (TGF-β), which is an anti-inflammatory cytokine secreted by M2 phenotype macrophage [44] (Fig. 2D).

In the AAD progression, a typical inflammatory response is usually initiated by the crosstalk between MAECs and MBMMs/monocytes involving MBMM/monocytes adhesion and pro-inflammatory polarization by aging MAECs. To investigate the effect of silicate ions derived from $CaSiO_3$ bioceramics on the crosstalk between MAECs and immune cells, we conducted two co-culture modes. In the direct contact co-culture model, MAECs were pretreated with CS or Ctrl for 72 h with or without LPS, then MBMMs or monocytes were added and co-cultured with MAECs for 1 h (Fig. 2E). The count of MBMMs adhered to the CS (52 ± 6 counts/field) treated MAECs without LPS induction was only about half of that in the Ctrl group (95 ± 9 counts/field) (Fig. S3). Also, a similar suppression effect of silicate ions on monocytes (THP-1 cells) attaching to LPS stimulated MAECs was observed in Fig. 2F, indicating an inhibiting effect of silicate ions on MAEC triggered MBMM/monocyte infiltration. In the indirect contact co-culture model, MAECs were pretreated with Ctrl or CS for 72 h, then the conditioned medium from MAECs was used to culture MBMMs for 48 h (Fig. 2G). The flow cytometric analysis exhibited that the percentage of $CD206^+$ $F4/80^+$ subpopulation were significantly increased from 3.68 ± 0.67% to 49.54 ± 8.93% when MBMMs were cultured in CS treated MAECs-conditioned

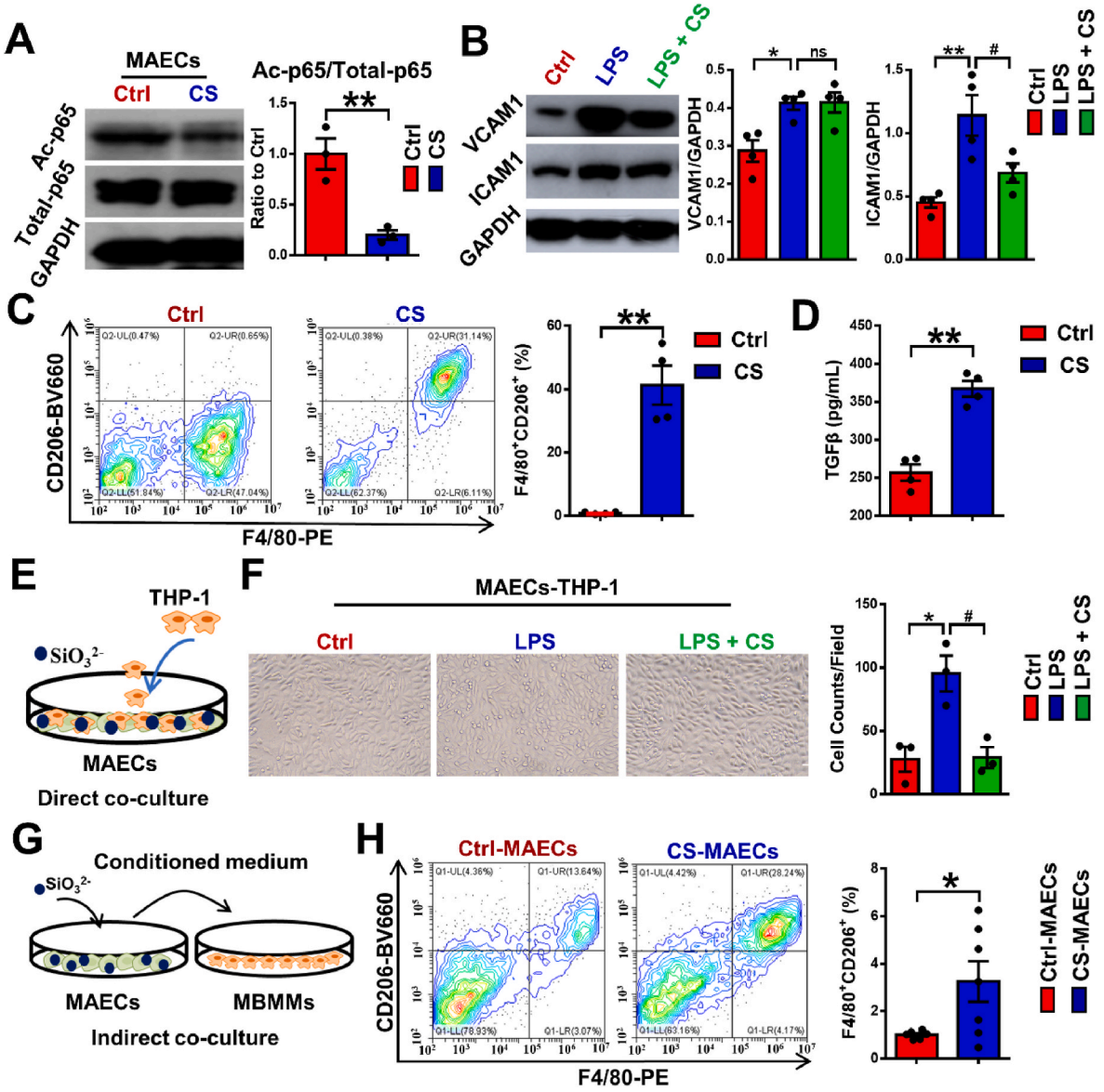

Fig. 2. Silicate ions as soluble form of bioactive ceramics alleviate inflammation of MAECs and MBMMs. (A) Representative Western blot of acetylated p65 (inflammation-associated protein, Ac-p65) and quantitative analysis of protein levels presented as mean ratio values quantified from protein bands of Ac-p65 versus total p65 (Total-p65) in cultured MAECs treated with Ctrl (n = 3) or CS (n = 3) for 72 h. (B) Representative Western blots of ICAM1 and VCAM1 (inflammation-associated proteins) and their quantitative analysis of protein levels represented as mean ratio values quantified from protein bands of ICAM1 and VCAM1 versus GAPDH in cultured MAECs treated with Ctrl, LPS or LPS + CS (n = 5). (C) Representative flow cytometric analysis of MBMM polarization and quantitative analysis of MBMM polarization (presented as the percentage of $CD206^+$ $F4/80^+$ cells) treated with Ctrl (n = 4) or CS (n = 4) for 72 h using phenotypic markers F4/80 (M0) and CD206 (M2). (D) The secreted TGF-β levels detected by Elisa assay in cultured MBMM conditioned medium treated with Ctrl (n = 4) or CS (n = 4) for 72 h. (E) Schematic diagram of direct contact coculture model: MAECs were pretreated with Ctrl or CS for 72 h, then MBMMs were added and co-cultured with MAECs for 1 h. (F) Representative images and quantitative cell count of THP-1 adhered to MAECs pretreated with Ctrl, LPS or LPS + CS in direct contact co-culture model. (n = 3). Scale bar, 100 μm. (G) Schematic diagram of indirect contact co-culture model: MAECs were pretreated with Ctrl or CS for 72 h, then the conditioned medium was used to culture MBMMs for 48 h. (H) Representative flow cytometric images and quantitative analysis of MBMM polarization (presented as the percentage of $CD206^+$ $F4/80^+$ cells) treated with conditioned medium from Ctrl pretreated MAECs or CS pretreated MAECs (n = 4) using phenotypic markers F4/80 (M0) and CD206 (M2) in indirect contact co-culture model. MBMMs, mouse bone marrow-derived macrophages. All data are presented as mean ± SEM. Statistical analysis was performed using (A, C, E, G and H) unpaired Student's t-test, (B and F) one-way ANOVA *P < 0.05 or **P < 0.01 vs. Ctrl, #P < 0.01 vs. LPS. ns: no significant difference.

medium (CS-MAECs) (Fig. 2H), indicating the suppression effect of silicate ions on MAEC triggered MBMM inflammation. All these results suggested that silicate ions derived from $CaSiO_3$ bioceramics alleviated MAECs inflammation, suppressed MBMMs/monocytes adhered to MAECs and promoted polarization of MBMMs towards M2 phenotype directly or by cell crosstalk.

3.3. *Silicate ions derived from $CaSiO_3$ bioceramics reduce the apoptosis of the mouse aortic smooth muscle cells (MASMCs)*

Apoptosis of aortic smooth muscle cells has been considered as a symptom of the later stage in AAD progression [45]. Therefore, we firstly investigated whether the silicate ions could regulate the apoptosis of smooth muscle cells directly. The anti-apoptosis effect of silicate ions on MASMCs was evaluated with or without Ang II treatment by flow cytometric analysis using apoptotic marker Annexin V-FITC and cell

viability dye propidium iodide (PI). The results showed that the untreated MASMCs have a certain degree of apoptosis, and after the Ang II treatment, the percentage of the apoptotic MASMCs were significantly increased, while silicate ions dramatically decreased the percentage of the apoptotic MASMCs for both untreated (Fig. S4) and Ang II treated cells (Fig. 3Aand S5). To confirm the result, the expressions of apoptotic markers (cleaved-caspase3 and cleaved-caspase9) of MASMCs were further assessed using WB assay. Both proteins were significantly decreased in CS treated MASMCs as compared to the Ctrl group (Fig. 3B), which was corresponding with the results of flow cytometric analysis.

Apart from the programmed apoptosis of MASMCs, inflammation initiated MASMC apoptosis plays an important role in AAD progression, which is usually mediated by the crosstalk between MASMCs and MBMMs including MBMM infiltration into the aortic tunica media driven by the inflammatory cytokines (e.g., VCAM1) secreted from MASMCs, and the induction of MASMC apoptosis triggered by the overproduced cytokines (e.g., TNF-α) from MBMMs [13,46]. To investigate the crosstalk between MASMCs and MBMMs, we conducted two co-culture modes. In the direct contact co-culture model, MASMCs were pretreated with CS for 72 h, then MBMMs were added and co-cultured with MASMCs for 1 h in order to determine the inhibitory effect of CS on MBMM adhesion through regulation of MASMCs (Fig. 3C). As shown in Fig. 3D, silicate ions significantly diminished the count of MBMMs adhered to MASMCs as only 85 ± 10 cells/field adhesion in CS group compared with Ctrl (143 ± 5 cells/field), indicating a suppression effect of silicate ions on MBMM infiltration. In the indirect contact co-culture model, MBMMs were pretreated with Ctrl or CS for 72 h, then the conditioned medium from MBMMs was used to culture MASMCs for 48 h (Fig. 3E). The flow cytometric analysis showed that the apoptosis of MASMCs was significantly decreased from 21.23 ± 0.65% to 14.92 ± 0.61% after the treatment with MBMMs-conditioned medium with CS pretreatment (CS-MBMMs) (Fig. 3F), indicating a suppression effect of silicate ions on MBMM induced MASMC apoptosis. All these results demonstrated that silicate ions derived from $CaSiO_3$ bioceramics could inhibit the apoptosis of smooth muscle cells directly or by cell crosstalk.

3.4. Silicate ions derived from $CaSiO_3$ bioceramics alleviate the AAD progression in the Ang II-induced AAD model

To verify our hypothesis that silicate ions may play a vital role in the effective treatment of AAD, we established a classical Ang II-induced AAD model in mice. Ang II is a common reagent for inducing AAD in rodents, which causes the occurrence of AAD (mainly occurs in abdominal aorta) through hyper lipid metabolism abnormalities and hemodynamic changes [13]. Briefly, 49-day-old male mice were fed a high-fat diet (HFD) and then implanted with osmotic pumps containing Ang II (1.44 mg/kg/day) or PBS at day 56 for 28 days. Silicate ion-containing saline (silicate ion concentration: 77.6 ± 0.16 μg mL^{-1}) or saline control (silicate ion concentration: 0.16 ± 0.01 μg mL^{-1}) were intravenously injected in mice 7 times every other day after 7 days' Ang II or PBS infusion. Experimental groups are defined as Ang II + Saline and Ang II + CS, respectively, and PBS pumping plus saline injection was used as control (PBS + Saline) (Fig. 4A). Firstly, the heart rate and blood pressure (BP) including the systolic BP, diastolic BP, and mean BP of mice after different treatments were evaluated. As shown in Fig. S6, both heart rate and BP showed a significant increase after Ang II infusion for 28 days as compared to the control group, while no significant differences of those parameters were observed between Ang II + Saline group and Ang II + CS group, indicating that silicate ions do not affect the heart rate and BP. The mice mortality rate displayed a mild decrease from 54.5% (6 death of 11, in Ang II + Saline group) to 45.5% (5 death of 11, in Ang II + CS group) after silicate ions treatment (Fig. 4B). Interestingly, although the AAD incidence rate was identical in both Ang II + Saline group and Ang II + CS group (100%, 11 out of 11), the severity of AAD was significantly relieved in Ang II + CS group as compared to Ang II + Saline group (Fig. 4C). The ultrasound (US) imaging analysis confirmed the results as Ang II infusion for 28 days

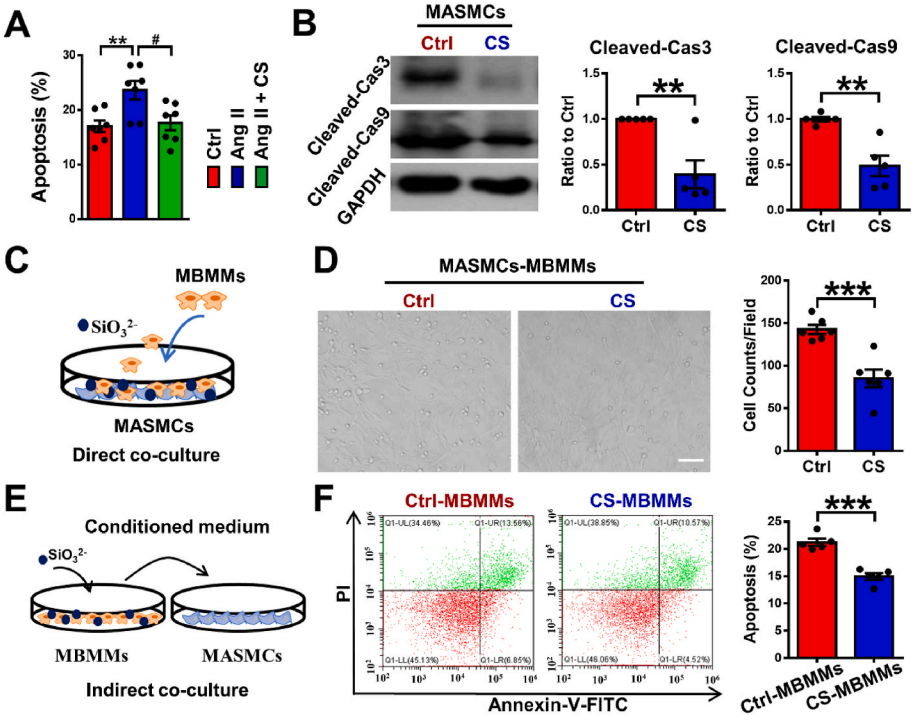

Fig. 3. Silicate ions as soluble form of bioactive ceramics reduce MASMC apoptosis. (A) Flow cytometric quantification analysis of apoptosis in MASMCs after treatment with Ctrl, Ang II or Ang II + CS using Annexin V-FITC and PI. (n = 7) (B) Representative Western blots of Cleaved-Cas3 and Cleaved-Cas9 (apoptotic-associated proteins) and their quantitative analysis of protein levels presented as mean ratio values quantified from protein bands of Cleaved-Cas3 and Cleaved-Cas9 versus GAPDH in cultured MASMCs treated with Ctrl (n = 5) or CS (n = 5) for 72 h. (C) Schematic diagram of direct contact co-culture model: MASMCs were pretreated with Ctrl or CS for 72 h, then MBMMs were added and cocultured with MASMCs for 1 h. (D) Representative images and quantitative cell counts of MBMMs adhered to MASMCs pretreated with Ctrl (n = 6) or CS (n = 6) in direct contact co-culture model. Scale bar, 100 μm. (E) Schematic diagram of indirect contact co-culture model: MBMMs were pretreated with Ctrl or CS for 72 h, then the conditioned medium was used to culture MASMCs for 48 h. (F) Representative flow cytometric images and quantitative analysis of MASMC apoptosis (presented as the percentage of Annexin V^+ cells) treated with conditioned medium from Ctrl pretreated MBMMs (Ctrl-MBMMs, n = 5) or CS pretreated MBMMs (CS-MBMMs, n = 5) using apoptotic markers Annexin V-FITC and PI in indirect contact co-culture model. MASMCs, mouse aorta smooth muscle cells. All data are presented as mean ± SEM. Statistical analysis was performed using (A) one-way ANOVA, (B–F) unpaired Student's t-test, $^{**}P < 0.01$, $^{***}P < 0.001$ vs.Ctrl, $^{\#}P < 0.01$ vs. Ang II.

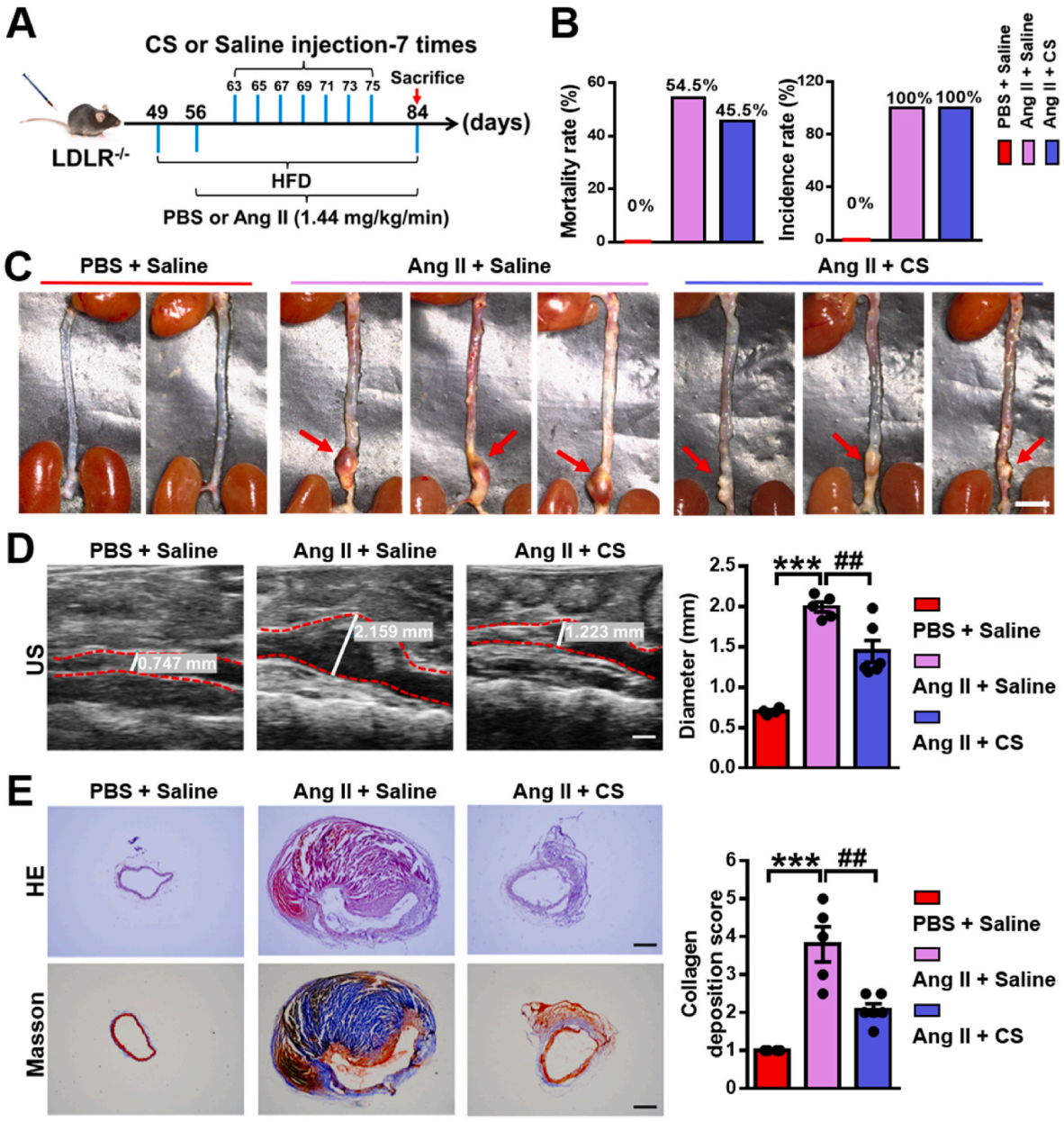

Fig. 4. Silicate ions as soluble form of bioactive ceramics reduce the aortic dilation and collagen deposition of abdominal aorta in the Ang II-induced AAD model. (A) Schematic diagram of experimental design: 49-day-old mice were fed a high-fat diet and then implanted with osmotic pumps containing Ang II (1.44 mg/kg/day) or PBS at day 56 for 28 days. Silicate ions-containing saline or saline control were intravenously injected into mice 7 times (every other day) after 7 days' Ang II or PBS infusion. Experimental groups were designated as Ang II + Saline, and Ang II + CS, respectively, and PBS pumping plus saline injection were used as control (PBS + Saline). (B) The mortality rate and AAD incidence rate after different treatments (n = 5 for PBS + Saline, n = 11 for Ang II + Saline and Ang II + CS). (C) Representative photographs of the whole aortas after different treatments. Red arrows show AADs. (D) Representative ultrasound (US) images and quantified maximal diameters of abdominal aortas. White lines and values represent the maximal diameters of abdominal aortas (n = 4 for PBS + Saline, n = 5 for Ang II + Saline, and n = 6 for Ang II + CS). (E) Representative HE and Masson's trichrome staining images and summary collagen deposition score calculated from the Masson's trichrome staining (n = 4 for PBS + Saline, n = 5 for Ang II + Saline, and n = 6 for Ang II + CS). Scale bars, 5 mm (C), 1 mm (D) and 200 μm (E). All data are presented as mean ± SEM, one-way ANOVA, ***P < 0.001 vs. PBS + Saline, ##P < 0.01 vs. Ang II + Saline.

provoked a remarkable increase in the maximal diameter of abdominal aorta from 0.7 ± 0.02 mm to 1.99 ± 0.06 mm, which was greatly attenuated to 1.44 ± 0.13 mm after silicate ions treatment (Fig. 4D). Furthermore, the histological analysis of HE and Masson's trichrome staining was applied to show the aortic architectures in different groups, which were obviously protected by silicate ions treatment since the aortic architectures in Ang II + CS group were closer to the PBS + Saline group as compared to Ang II + Saline group. Also, significant inhibition of collagen deposition was observed after the treatment with silicate ions as the collagen deposition score calculated from the Masson's trichrome staining decreased from 3.8 ± 0.46 in Ang II + Saline group to 2.08 ± 0.15 in Ang II + CS group (Fig. 4E). Moreover, modified Gomori staining displayed the serious degradation of elastin laminae in abdominal aorta after Ang II infusion, and the results showed that the treatment of silicate ions decreased the percentage of grade IV (33.4%) as compared with Ang II + Saline group (60%), indicating a clear reduction of elastin laminae degradation of the abdominal aortas (Fig. S7). These results implied that silicate ions derived from $CaSiO_3$ bioceramics can attenuate the AAD progression by the inhibition of aortic dilation, collagen deposition, and elastin laminae degradation of

abdominal aorta.

To confirm the role of silicate ions derived from $CaSiO_3$ bioceramics in attenuating AAD progression, we further detected the senescence of aortas in different groups using SA-β-gal staining. The result showed that the SA-β-gal positive staining visibly appeared after the Ang II infusion and was significantly decreased after the treatment of silicate ions. The corresponding quantitative analysis confirmed the result as the percentages of the SA-β-gal positive areas were 0%, 19.3 ± 6.60%, and 4.46 ± 1.22% in the group of PBS + Saline, Ang II + Saline and Ang II + CS, respectively (Fig. 5A). Then, we examined the inflammation of aortas in different groups using immunohistochemical analysis of ICAM1 and VCAM1. As shown in Fig. 5B, the protein expression of both ICAM1 and VCAM1 were lower in abdominal aortas of Ang II + CS group as compared to Ang II + Saline group, and a significant reduction was observed in the expression of ICAM1. Finally, we evaluated the anti-apoptosis effect of silicate ions using immunohistochemical analysis of two apoptotic markers (caspase3 and caspase9). The expression of both caspase3 and caspase9 in the abdominal aorta was potently increased after Ang II infusion, while this increase was prominently reduced with the treatment of silicate ions (Fig. 5C). The immunofluorescence assay of TUNEL was further conducted, which verified the anti-apoptosis effect of silicate ions as much fewer apoptotic cells were observed in the abdominal aorta of Ang II + CS group (mean density value: 1.26 ± 0.28%) as compared with the Ang II + Saline group (mean density value: 11 ± 3.3%) (Fig. S8). These results indicated that silicate ions derived from $CaSiO_3$ bioceramics indeed attenuated the Ang II-induced AAD progression by inhibiting the senescence, inflammation, and apoptosis of aorta.

3.5. *Silicate ions derived from $CaSiO_3$ bioceramics alleviate the AAD progression in the β-BAPN induced AAD model*

To further confirm the therapeutic effect of silicate ions on AAD, we conducted a secondary classical AAD model induced by β-BAPN. β-BAPN is a lysyl oxidase inhibitor, which induces the occurrence of AAD (mainly occurs in aortic arch) by disrupting the cross-linking of elastin and collagen [47]. We firstly designed a treatment method of silicate ions similar to that implemented in the mentioned Ang II-induced AAD model above, termed as Design I. Briefly, 21-day-old male mice were administrated with β-BAPN (0.8 g/kg/day) containing water for 28 days, and followed with intravenous injection of silicate ions containing saline or saline control 7 times every other day after 7 days' β-BAPN administration (Fig. 6A). The experimental groups were defined as β-BAPN + Saline, and β-BAPN + CS, respectively, and pure water feeding plus saline injection was used as control (H_2O + Saline). As shown in Fig. 6B, the mice mortality rate was mildly decreased from

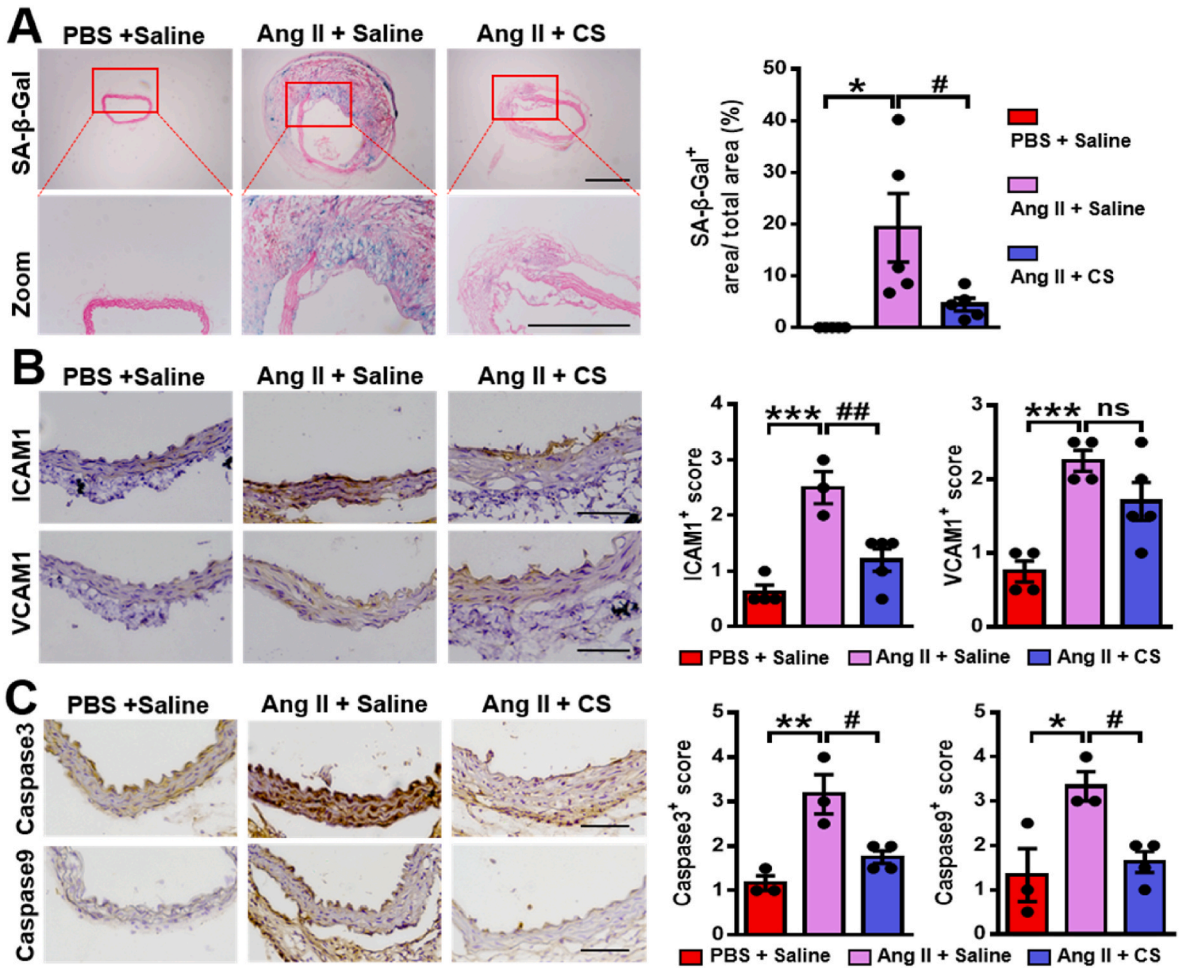

Fig. 5. Silicate ions as soluble form of bioactive ceramics reduce senescence, inflammation, and cell apoptosis of the aortas in the Ang II-induced AAD model. (A) Representative images of SA-β-gal positive staining (blue) and quantitative results (presented as percentage SA-β-gal positive area versus total area) in abdominal aortas. Red boxed areas are expanded to show representative high-power fields (n = 4 for PBS + Saline, n = 5 for Ang II + Saline and Ang II + CS). (B) Representative immunohistochemistry images and summary scores of inflammation-associated proteins ICAM1 and VCAM1 in abdominal aortas after different treatments (n = 4 for PBS + Saline, n = 3 for Ang II + Saline, and n = 5 for Ang II + CS). (C) Representative immunohistochemistry images and summary scores of caspase 3 and caspase 9 (apoptosis-associated proteins) in abdominal aortas (n = 3 for PBS + Saline and Ang II + Saline, and n = 4 for Ang II + CS). Scale bars, 200 μm (A), and 100 μm (B and C). All data are presented as mean ± SEM, one-way ANOVA. *P < 0.05, **P < 0.01 or ***P < 0.001 vs. PBS + Saline, #P < 0.05 or ##P < 0.01 vs. Ang II + Saline.

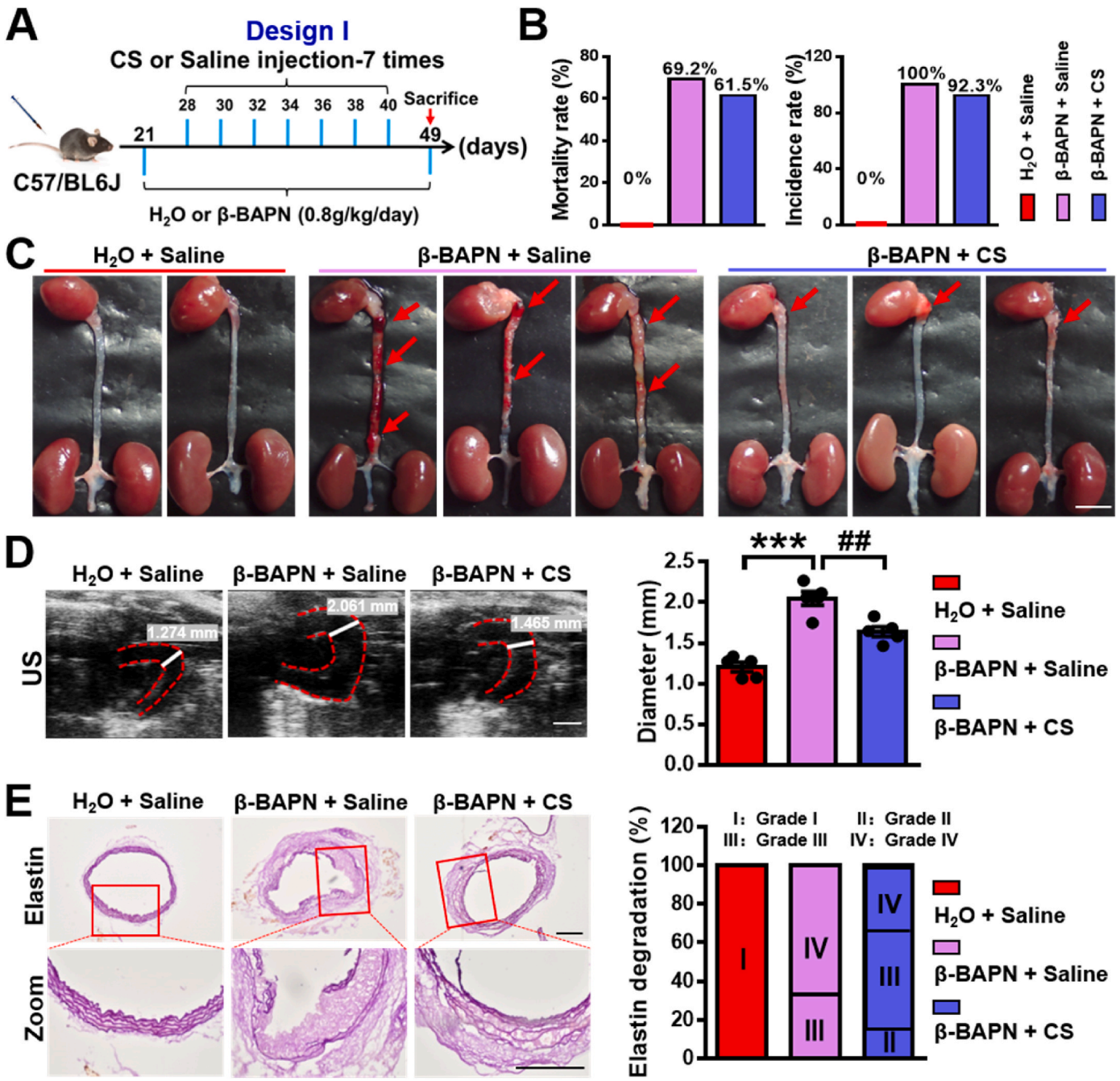

Fig. 6. Silicate ions as soluble form of bioactive ceramics administrated in the mode of Design I suppress β-BAPN induced AAD formation: reducing mortality rate and AAD incidence rate as well as inhibiting the aortic dilation and elastin laminae degradation of the aortic arches. (A) Schematic diagram of treatments in Design I: 21-day-old mice were administrated with β-BAPN (0.8 g/kg/day) containing water or free water for 28 days. Silicate ions-containing saline or saline control were intravenously injected in mice 7 times (every other day) after 7 days' β-BAPN administration. Experimental groups were designated as β-BAPN + Saline and β-BAPN + CS, respectively, and pure water feeding plus saline injection were used as control (H_2O + Saline). (B) The mortality rate and AAD incidence rate after different treatments (n = 5 for H_2O + Saline, n = 13 for β-BAPN + Saline and β-BAPN + CS). (C) Representative photographs of whole aortas in Design I. Red arrows show AADs. (D) Representative US images and quantitative maximal diameters of aortic arches in Design I. White lines and values represent the maximal diameters of aortic arches (n = 5 for H_2O + Saline, β-BAPN + Saline, and β-BAPN + CS). (E) Representative photographs and quantification of the percentage of different degrees of the elastin laminae degradation in aortic aortas using modified Gomori staining in Design I. Red boxed areas are expanded to show representative high-power fields. Elastin laminae gradation grades: intact internal elastic lamina (I), mild elastin fragmentation (II), severe elastin digestion (III), and severe elastin digestion with a visible ruptured site (IV). (n = 3 for H_2O + Saline, n = 6 for β-BAPN + Saline and β-BAPN + CS). Scale bars, 5 mm (C), 2 mm (D) and 500 μm (E). Data are presented as mean ± SEM, one-way ANOVA, $^{***}P < 0.001$ vs. H_2O + Saline, $^{\#\#}P < 0.01$ vs. β-BAPN + Saline.

69.2% (9 death of 13, in β-BAPN + Saline group) to 61.5% (8 death of 13, in β-BAPN + CS group) and the AAD incidence rate declined from 100% (13 out of 13, in β-BAPN + Saline group) to 92.3% (12 out of 13, in β-BAPN + CS group) after the treatment of silicate ions. Although the reduction of mortality rate or AAD incidence rate was gentle after the administration of silicate ions, the progression of AAD was apparently depressed as much less severe AADs were observed in β-BAPN + CS group as compared to β-BAPN + Saline group (Fig. 6C). The maximal diameter of aortic arch was calculated from US images, which was 1.21 ± 0.06 mm, 2.05 ± 0.08 mm, and 1.64 ± 0.06 mm in the groups of H_2O

+ Saline, β-BAPN + Saline, and β-BAPN + CS, respectively. (Fig. 6D). To determine the degradation of elastin laminae in different groups, modified Gomori staining was conducted. The result displayed that the elastin laminae degradation in aortic arch was serious in β-BAPN + Saline group, and this effect was visibly reversed with the treatment of the silicate ions as the percentage of grade IV were 0, 66.7% and 33.3% in H_2O + Saline, β-BAPN + Saline and β-BAPN + CS, respectively. (Fig. 6E). To verify the crucial role of silicate ions on the regulation of inflammatory response in AAD progression, we further detected macrophage accumulation (F4/80-positive cells) in aortic arches among different groups. The results showed that much fewer macrophages were observed in the aortic wall in β-BAPN + CS group as compared to the β-BAPN + saline group, indicating that silicate ions reduced the macrophage infiltration into the aortic wall (Fig. S9A). Moreover, the immunohistochemistry assay of ICAM1 and VCAM1 (Fig. S9B) further confirmed the anti-inflammatory effect of silicate ions since the expression of ICAM1 in aortic arches was significantly decreased in the β-BAPN + CS group as compared to β-BAPN + saline group. Finally, the immunofluorescence assay of TUNEL was applied to investigate the anti-apoptosis effect of silicate ions. A dramatic decline of the mean

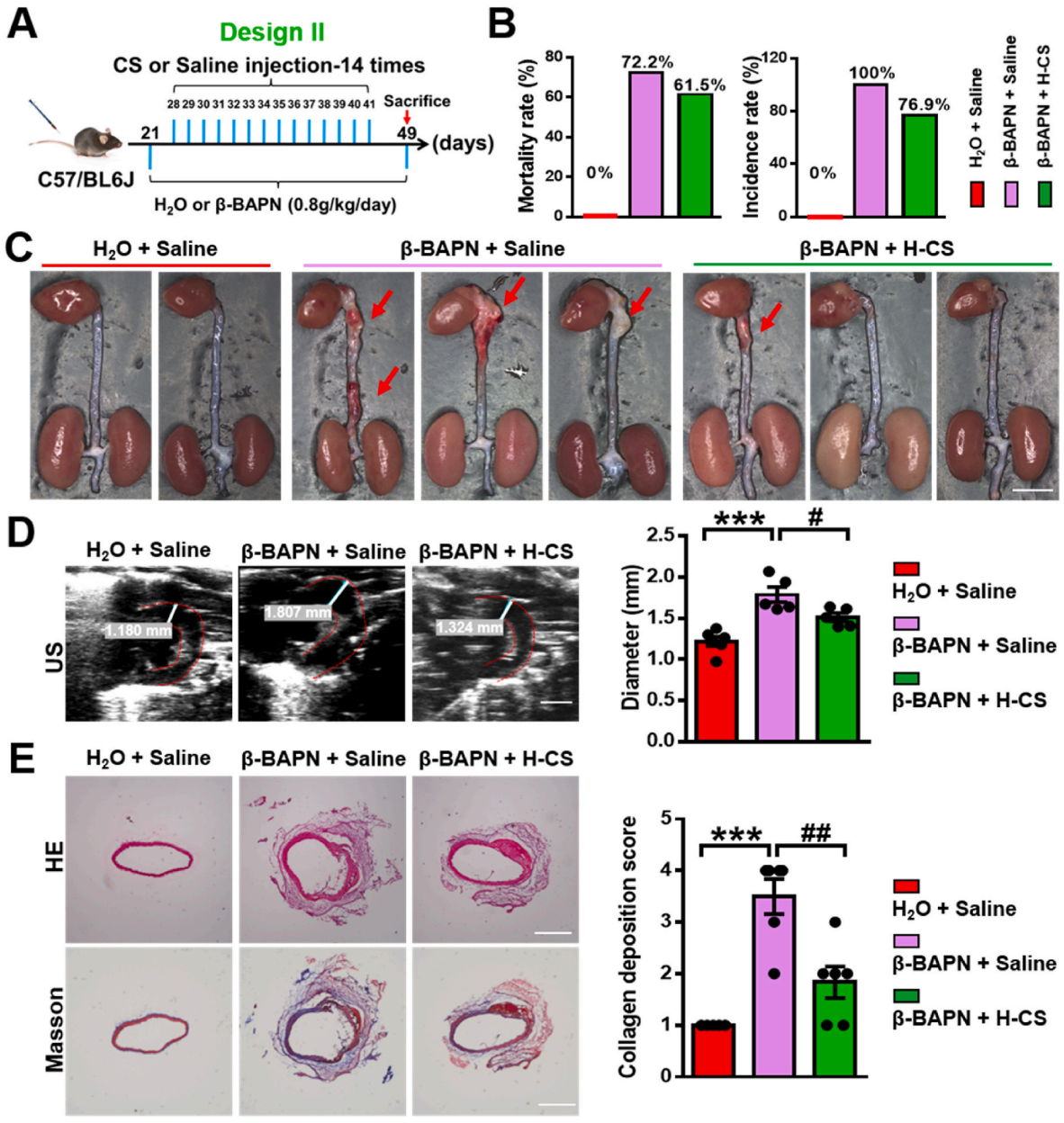

Fig. 7. Silicate ions as soluble form of bioactive ceramics administrated in the mode of Design II suppress β-BAPN induced AAD formation: reducing mortality rate and AAD incidence rate as well as inhibiting the aortic dilation and collagen deposition of the aortic arches. (A) Schematic diagram of treatments in Design II: 21-day-old mice were administrated with β-BAPN (0.8 g/kg/day) containing water or free water for 28 days. Silicate ions-containing saline or saline control were intravenously injected in mice 14 times every day after 7 days' β-BAPN administration. Experimental groups were designated as β-BAPN + Saline and β-BAPN + H-CS, respectively, and pure water feeding plus saline injection were used as control (H_2O + Saline). (B) The mortality rate and AAD incidence rate after different treatment (n = 6 for H_2O + Saline, n = 18 for β-BAPN + Saline, and n = 13 for β-BAPN + CS). (C) Representative photographs of whole aortas in Design II. Red arrows show AADs. (D) Representative US images and quantitative maximal diameters of aortic arches in Design II. White lines and values represent the maximal diameters of aortic arches (n = 5 for H_2O + Saline, β-BAPN + Saline, and β-BAPN + CS). (E) Representative HE and Masson's trichrome staining images and summary collagen deposition score of aortic arches (n = 4 for H_2O + Saline, n = 4 for β-BAPN + Saline, and n = 6 for β-BAPN + CS). Scale bars, 2 mm (C), 1 mm (D) and 200 μm (E). All data are presented as mean ± SEM, one-way ANOVA. ***P < 0.001 vs. PBS + Saline, $^{\#}$P < 0.05 or $^{\#\#}$P < 0.01 vs. β-BAPN + Saline.

fluorescence density value (from 4.52 ± 0.95 to 1.97 ± 0.32) was shown in the β-BAPN + CS group as compared to β-BAPN + Saline group (Fig. S10), indicating much fewer apoptotic cells in the aortic arches after the treatment of silicate ions. All these results clearly revealed the beneficial effect of silicate ions derived from $CaSiO_3$ bioceramics against β-BAPN induced AAD progression.

Then, we further investigated the dose-dependency of silicate ions treatment by designing another animal experiment with increased treatment times using the same β-BAPN induced AAD model, termed as Design II. Briefly, 21-day-old male mice were administrated with β-BAPN (0.8 g/kg/day) containing water for 28 days. Then, silicate ions containing saline were intravenously injected in mice every day for 14 times after 7 days' β-BAPN administration (Fig. 7A). The experimental groups were defined as β-BAPN + Saline and β-BAPN + H-CS, respectively, and pure water feeding plus saline injection was set as control (H_2O + Saline). As shown in Fig. S11, A and B, there were no significant differences in the heart rate and BP among the three groups. However, silicate ions employment decreased the mice mortality rate from 72.2% (13 death of 18, in β-BAPN + Saline group) to 61.5% (8 death of 13, in β-BAPN + H-CS group). Also, the AAD incidence rate declined from 100% (18 out of 18, in β-BAPN + Saline group) to 76.9% (10 out of 13, in β-BAPN + H-CS group) after the treatment of enhanced silicate ions (Fig. 7B). It is worth mentioning that the reduction of mice mortality rate increased from 7.7% (in design I) to 10.7% (in design II) with increased dosage (treatment times) of silicate ion treatment. Also, the reduction of AAD incidence rate increased from 7.7% (in design I) to 23.1% (in design II), confirming that the increased dosage of silicate ions further improved the therapeutic effects and decreased both mortality and AAD incidence rate (Fig. S12 A and B). Similar to the results of design I, the severity of AAD was significantly alleviated in the β-BAPN + H-CS group as compared to the β-BAPN + saline group, shown by the representative photographs of whole aortas in Fig. 7C. The maximal aortic arch diameter was significantly decreased in the β-BAPN + H-CS group (1.51 ± 0.05 mm) as compared to the β-BAPN + saline group (1.79 ± 0.09 mm) calculated from US images of aortic arches (Fig. 7D). Moreover, as shown in Fig. 7E, the histological analysis of HE and Masson's trichrome staining demonstrated that the aortic architectures in β-BAPN + H-CS group were more integrated with less collagen deposition as compared to that in the β-BAPN + saline group considering the collagen deposition score decreased from 3.5 ± 0.34 to 1.83 ± 0.31 after the treatment of silicate ions. The modified Gomori staining displayed more elastin laminae degradation in aortic arch after β-BAPN infusion and this effect was reversed with the silicate ions treatment as the percentage of grade IV were 0, 83% and 0% in H_2O + Saline, β-BAPN + Saline and β-BAPN + H-CS, respectively (Fig. S13A). To affirm the anti-senescence effect of silicate ions, the SA-β-gal staining was conducted, and representative images and the corresponding quantitative analysis exhibited that the percentage of SA-β-gal positive area in the aortic arch was significantly reduced from 25.58 ± 4.29% to 4.05 ± 2.64 after the treatment of silicate ions (Fig. S13B). All these data denoted that the effect of silicate ions derived from $CaSiO_3$ bioceramics on AAD is dose-dependent, and increased administration of silicate ions may improve the therapeutic effects against AAD progression.

After the investigation of the therapeutic effect of silicate ions, we examined the biosafety of silicate ions for AAD treatment in the model of design II, we performed the histological analysis of crucial organs including the heart, kidneys, liver, lungs, and spleen among different groups. Gross pathological and histopathological examination revealed that there was no sign of structural abnormalities were observed in β-BAPN + Saline and β-BAPN + H-CS groups as compared to H_2O + Saline group (Fig. S14). This finding indicated the biosafety of "silicate ion therapy".

4. Discussion

Aging plays a vital role in CVDs, especially in the development of AAD [38,48]. The over-released inflammatory factors from senescent ECs may cause immune cells infiltration as well as abnormal apoptosis of SMCs, resulting in the formation of AAD [37,49,50]. Since the development of AAD results from comprehensive effects of multiple cellular processes [51,52], the therapeutic approaches only targeting a single type of cells or one signaling pathway might have limited effectiveness and be unable to solve the problem fundamentally. Based on our previous studies that calcium silicate bioactive ceramics can regulate cellular behaviors of various types of cells (e.g., ECs [53], cardiomyocytes [35,54], mesenchymal stem cells [55,56] and macrophages [57]), and their interactions (EC-cardiomyocytes [35], EC-macrophages [58], and macrophage-mesenchymal stem cell [25], etc.), we proposed a "silicate ion therapy" to systemically regulate the local aortic microenvironment, aiming at the three main stages of the AAD progression, including EC senescence, immune cells infiltration, and SMC apoptosis. Unlike traditional interventions that only target a specific type of cells, a specific signaling pathway or a particular phase of AAD, our results revealed that silicate ions could concurrently regulate a variety of cells (MAECs, MBMMs, and MASMCs) involved in AAD occurrence and attenuate AAD progression through constraining senescence, inflammation, and cell apoptosis of aorta in both Ang II and β-BAPN induced AAD mouse models (Fig. 8).

Since vascular senescence is a crucial factor relevant to the occurrence of AAD, alleviating the senescence of the aorta may reduce the development of AAD. Previous studies have shown that silicon supplementation can prevent age-related alterations in the endothelium-dependent vascular relaxation through increasing the expression of nitric oxide synthase and aquaporin-1 [59]. However, it is unknown whether and how silicate ions can inhibit aorta senescence at cellular level. Our previous studies have demonstrated the bioactivity of silicate ions released from $CaSiO_3$ bioceramics could activate ECs and enhance various cellular functions, such as stimulation of proliferation, up-regulation of pro-angiogenic factors (e.g., vascular endothelial growth factor and vascular endothelial growth factor receptor) in vascular ECs [35]. Inspired by these findings, we think that silicate ions might be capable to delay the senescence of aortic ECs (AECs). In this study, we first explored the anti-senescence ability of silicate ions on MAECs *in vitro* and found that the treatment of silicate ions indeed significantly reduced the proportion of senescent MAECs (positive for SA-β-Gal), accomplished with up-regulated expression of longevity regulator SIRT1 and inhibited the nucleation of DNA damage marker γH2A.X. The further *in vivo* studies verified that silicate ions derived from $CaSiO_3$ bioceramics significantly reduced the SA-β-Gal expression in aortas in both Ang II and β-BAPN induced AAD mouse models, indicating the potential role of silicate ions in alleviating vascular aging. We believe that these findings exhibit great significance not only for the prevention and treatment of AAD, but also for the intervention of other aging-related vascular diseases, although further extensive studies are required to investigate the anti-senescence effect of bioactive ions for other vascular tissues.

In addition to delaying the senescence of AECs, inhibiting apoptosis of aortic smooth muscle cells (ASMCs) is also a critical approach to resist the progression of AAD [60,61]. ASMCs are highly plastic arterial vascular cells located in the media of aorta, which coordinate the function of vasoconstriction/vasodilatation and maintain vascular tension and elasticity [62]. The abnormal apoptosis of ASMCs is a typical pathological feature of AAD formation [63]. Therefore, inhibition of ASMC apoptosis might be an efficient therapeutic strategy for the treatment of AAD. Our previous studies have shown that silicate ions derived from $CaSiO_3$ bioceramic can inhibit apoptosis of various cells, including cardiomyocytes [35], and macrophages [24]. However, it is still unknown whether silicate ions have anti-apoptosis effect on ASMCs. In this study, we first found that silicate ions derived from $CaSiO_3$ bioceramic reduced the apoptosis and expression of apoptosis-related proteins (cleaved-caspase 3 and cleaved-caspase 9) in cultured MASMCs, indicating that silicate ions could not only affect the senescence of AECs,

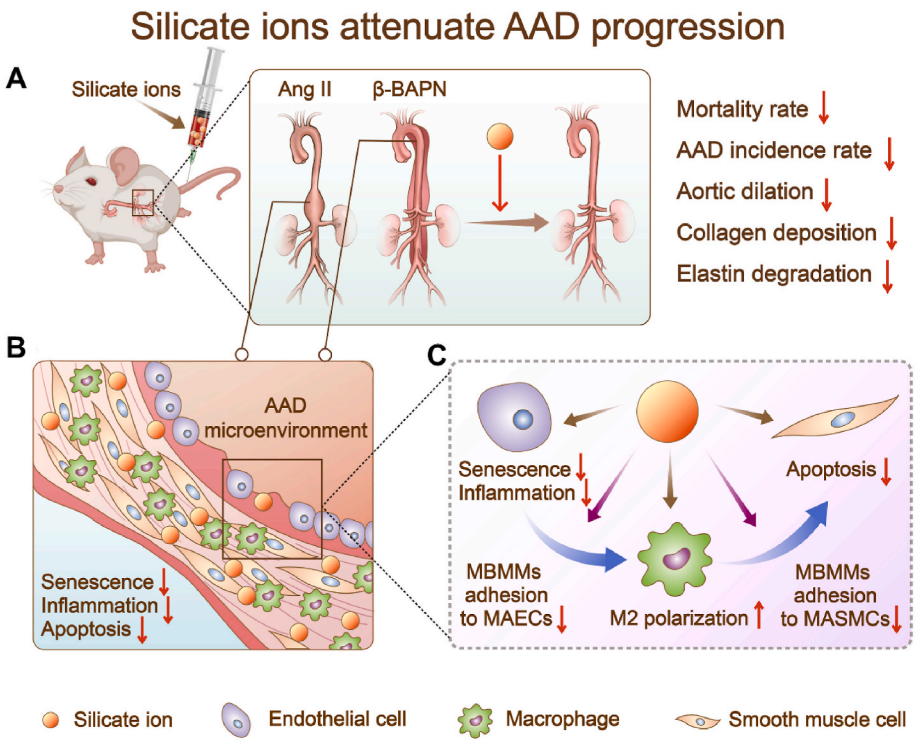

Fig. 8. Scheme describing the "silicate ion therapy" on AAD. (A) Intravenous injection of silicate ions as soluble form of bioactive ceramics attenuates both Ang II and β-BAPN induced AAD progression, including reduced mortality rate, AAD incidence rate, aortic dilation, collagen deposition and elastin degradation. (B) Silicate ions as soluble form of bioactive ceramics modulate the vascular microenvironment by inhibiting senescence, inflammation, and apoptosis of aorta. (C) Silicate ions as soluble form of bioactive ceramics alleviate MAEC senescence and inflammation, promote polarization of MBMMs towards M2 phenotype, inhibit the adhesion of MBMMs to MAECs (or MASMCs) and the apoptosis of MASMCs directly or by mediating cell-cell crosstalk.

but also protect ASMCs from apoptosis. One possible mechanism is that silicate ions may inhibit cell apoptosis through regulating apoptotic-associated ERK1/2 and p38 MAPK signaling pathways, which was proved in our previous study as silicate ions could alleviate the glucose/oxygen deprivation induced cell apoptosis by stimulating the expression of phosphorylated ERK1/2 and decreasing the expression of phosphorylated p38 in NRCMs, respectively [35]. Further *in vivo* experiments confirmed the effect of silicate ions in reducing the apoptotic cell proportion in aorta during the progression of AAD. These results suggest that the dual-functional regulation of two different types of cells (AECs and ASMCs) is possible by silicate ions, which may contribute to the enhanced therapeutic effect in the treatment of AAD.

The pathogenesis of AAD is extremely complex, which involves a variety of cellular processes. Besides AEC injury and ASMC apoptosis, the excessive participation of immune cells is also a key factor to the formation of AAD [44,64]. A typical AAD development process is usually initiated by the dysfunction of ECs, which secret abundant inflammatory factors to trigger immune cells infiltration [65]. The adhered immune cells release a series of proteolytic enzymes (e.g., matrix metalloproteinases) [66] or differentiated towards M1 phenotype to produce pro-apoptotic factors (e.g., TNF-α) [44], which eventually cause the apoptosis of ASMCs and induce the formation of AAD. Therefore, the regulation of macrophage/monocyte adhesion to MAECs (or MASMCs) and macrophage polarization are the important therapeutic target for the treatment of AAD. Although many drugs (e.g., statins) have been reported to promote macrophages to M2 polarization [67], no satisfactory therapeutic effect has been shown in the clinical trials, which suggests that this kind of single-target approach might not be effective enough to inhibit AAD progression. In fact, the initiation and progression of AAD are the results of multiple cell and cell-cell communications including macrophage-AECs and macrophage-ASMCs interactions [51]. However, limited attention has been paid to the interaction of the immune cells and aortic related cells. In contrast to the single-target approach for macrophage polarization, our study found that silicate ions can not only directly promote M2 polarization of MBMMs, reduce inflammation of MAECs and apoptosis of MASMCs, but also regulate the interaction between MAECs (or MASMC) and MBMMs/monocytes, and systematically improve the local microenvironment for vascular repairing. It is worth noting that, to explore the anti-adhesion effect of silicate ions on early or late immune cells, we detect the adhesion ability of macrophages and monocytes to MAECs, respectively. We found that silicate ions could decrease the adhesion of both macrophages and monocytes to MAECs simultaneously. Furthermore, we found that silicate ions can reduce the secretion of inflammatory cytokines ICAM1 in MAECs. Such an inhibitory effect is usually achieved by regulating the inflammation-related NF-κB signal pathway in ECs and significantly contributes to the enhanced M2 polarization of MBMMs via paracrine mechanisms. Also, our *in vitro* data revealed that silicate ions derived from $CaSiO_3$ bioceramics can reduce the adhesion of MBMMs to MAECs and MASMCs, which might be the reason why silicate ions diminish macrophage aggregation and excessive infiltration in aortic walls. Moreover, such alleviated macrophage infiltration and reduced adhesion on ASMCs further depressed the apoptosis of ASMCs and attenuated the progression of AAD. These results suggest that silicate ions derived from $CaSiO_3$ bioceramics can regulate the interaction between vascular-related cells and macrophages, benefit the local microenvironment of aortas, and inhibit the occurrence and development of AAD through immune regulation and paracrine mechanisms.

It is worth mentioning that in the present study we applied silicate ions through dissolution of $CaSiO_3$ bioceramics, which is critical for the application of ion therapy. The extracts of $CaSiO_3$ bioceramics consist of calcium and silicate ions, and theoretically, a solution with same calcium and silicate ion concentration might be obtained by using solutions of soluble calcium salt and silicate. However, the solution of soluble calcium salt such as calcium chloride, and the only soluble silicate, namely sodium silicate, contains not only calcium and silicate ions, but also other cations and anions such as chloride and sodium ions, which may cause negative effects for therapy. So, one of the advantages of the application of bioactive silicate ceramics is that ionic solution with specific ion combinations and concentration can be obtained without unwanted ion contamination by selection of silicate bioactive ceramics with specific chemical composition. Therefore, although in the present study we used the simplest calcium silicate ceramic, it is possible to extend this approach by using bioactive silicate ceramics with different

compositions for treatment of other diseases which may need different silicate ion composition due to different pathogenesis.

5. Conclusions

Collectively, "silicate ion therapy" based on the application of bioactive ceramics in soluble form is proposed to treat AAD for the first time. Such a strategy focused on the systemic regulation of local vascular microenvironment, aiming to manipulate cells and cell-cell interactions in three main pathological stages of AAD simultaneously, including senescence, inflammation, and cell apoptosis of aorta. The *in vitro* studies demonstrated that injection of silicate ions derived from $CaSiO_3$ bioceramic alleviated MAEC senescence and inflammation, promote polarization of MBMMs towards M2 phenotype and inhibited the apoptosis of MASMCs directly or by mediating cell-cell crosstalk. Furthermore, the *in vivo* studies verified the therapeutic effect of the multiple comprehensive regulatory functions of silicate ions and demonstrated the effective prevention of the development of AAD induced in both Ang II and β-BAPN mouse models by alleviating the aortic dilation, collagen deposition, and elastin laminae degradation of aortas through the inhibition of aortic senescence, inflammation, and cell apoptosis. The therapeutic effect was dose-dependent, and an increased dose of treatment significantly reduced the mortality and AAD incidence rate. This proposed application of the soluble form of bioactive ceramics not only opens a new avenue for the treatment of AAD but might also be applied for the treatment of other aging-related vascular diseases.

Ethics approval and consent to participate

The animal protocol and experimental procedures of this study were approved by the Animal Research and Ethics Committee of Wenzhou Institute of University of Chinese Academy of Sciences (Approval Issue No. WIUCAS21061702 and WIUCAS20111901).

Declaration of competing interest

The authors declare that they have no conflict of interest.

Data availability statement

The raw/processed data forms part of an ongoing study and may be requested from the authors.

CRediT authorship contribution statement

Yumei Que: formulated the hypothesis and designed the research, performed the research and analyzed the data, wrote the manuscript. **Zhaowenbin Zhang:** performed the research and analyzed the data. **Yanxin Zhang:** performed the research and analyzed the data. **Xin Li:** performed the research and analyzed the data. **Likai Chen:** performed the research and analyzed the data. **Peier Chen:** performed the research and analyzed the data. **Caiwen Ou:** revised the manuscript. **Chen Yang:** formulated the hypothesis and designed the research, wrote the manuscript. **Jiang Chang:** formulated the hypothesis and designed the research, wrote the manuscript, revised the manuscript.

Acknowledgments

This work was supported by National Natural Science Foundation of China (82100427), the Strategic Priority Research Program of the Chinese Academy of Sciences (XDA16010203), the seed grants from the Wenzhou Institute, University of Chinese Academy of Sciences (WIUCASQD2020013, WIUCASQD2021030), and the founding from First Affiliated Hospital of Wenzhou Medical University.

Appendix A. Supplementary data

Supplementary data to this article can be found online at https://doi.org/10.1016/j.bioactmat.2022.07.005.

References

[1] United Nations Department Of Economic And Social Affairs, Population Division, The 2019 revision of world population Prospects. https://population.un.org/wpp/.
[2] B.J. North, D.A. Sinclair, The intersection between aging and cardiovascular disease, Circ. Res. 110 (8) (2012) 1097–1108, https://doi.org/10.1161/CIRCRESAHA.111.246876.
[3] D.P. Howard, A. Banerjee, J.F. Fairhead, A. Handa, L.E. Silver, P.M. Rothwell, S. Oxford Vascular, Age-specific incidence, risk factors and outcome of acute abdominal aortic aneurysms in a defined population, Br. J. Surg. 102 (8) (2015) 907–915, https://doi.org/10.1002/bjs.9838.
[4] T. Fukui, Management of acute aortic dissection and thoracic aortic rupture, J. Intensive. Care. 6 (2018) 15, https://doi.org/10.1186/s40560-018-0287-7.
[5] E. Bossone, K.A. Eagle, Epidemiology and management of aortic disease: aortic aneurysms and acute aortic syndromes, Nat. Rev. Cardiol. 18 (5) (2021) 331–348, https://doi.org/10.1038/s41569-020-00472-6.
[6] G. Gialdini, N.S. Parikh, A. Chatterjee, M.P. Lerario, H. Kamel, D.B. Schneider, B. B. Navi, S.B. Murthy, C. Iadecola, A.E. Merkler, Rates of spinal cord infarction after repair of aortic aneurysm or dissection, Stroke 48 (8) (2017) 2073–2077, https://doi.org/10.1161/STROKEAHA.117.017071.
[7] J. Chung, L.M. Stevens, M.W.A. Chu, F. Dagenais, M.D. Peterson, M. Boodhwani, J. Bozinovski, I. El-Hamamsy, M.H. Yamashita, R. Atoui, B. Bittira, D. Payne, M. Ouzounian, C. Canadian, Thoracic Aortic, the impact of age on patients undergoing aortic arch surgery: evidence from a multicenter national registry, J. Thorac. Cardiovasc. Surg. 162 (3) (2021) 759–766, https://doi.org/10.1016/j.jtcvs.2020.02.032.
[8] Y.H. Shen, S.A. LeMaire, N.R. Webb, L.A. Cassis, A. Daugherty, H.S. Lu, Aortic aneurysms and dissections series, Arterioscler. Thromb. Vasc. Biol. 40 (3) (2020) e37–e46, https://doi.org/10.1161/ATVBAHA.120.313991.
[9] A.J. Donato, D.R. Machin, L.A. Lesniewski, Mechanisms of dysfunction in the aging vasculature and role in age-related disease, Circ. Res. 123 (7) (2018) 825–848, https://doi.org/10.1161/CIRCRESAHA.118.312563.
[10] L.M. Fan, G. Douglas, J.K. Bendall, E. McNeill, M.J. Crabtree, A.B. Hale, A. Mai, J. M. Li, M.A. McAteer, J.E. Schneider, R.P. Choudhury, K.M. Channon, Endothelial cell-specific reactive oxygen species production increases susceptibility to aortic dissection, Circulation 129 (25) (2014) 2661–2672, https://doi.org/10.1161/CIRCULATIONAHA.113.005062.
[11] I. El-Hamamsy, M.H. Yacoub, Cellular and molecular mechanisms of thoracic aortic aneurysms, Nat. Rev. Cardiol. 6 (12) (2009) 771–786, https://doi.org/10.1038/nrcardio.2009.191.
[12] R.A. Quintana, W.R. Taylor, Cellular mechanisms of aortic aneurysm formation, Circ. Res. 124 (4) (2019) 607–618, https://doi.org/10.1161/CIRCRESAHA.118.313187.
[13] Y. Que, X. Shu, L. Wang, P. Hu, S. Wang, R. Xiong, J. Liu, H. Chen, X. Tong, Inactivation of cysteine 674 in the SERCA2 accelerates experimental aortic aneurysm, J. Mol. Cell. Cardiol. 139 (2020) 213–224, https://doi.org/10.1016/j.yjmcc.2020.02.003.
[14] J.P. Habashi, D.P. Judge, T.M. Holm, R.D. Cohn, B.L. Loeys, T.K. Cooper, L. Myers, E.C. Klein, G. Liu, C. Calvi, M. Podowski, E.R. Neptune, M.K. Halushka, D. Bedja, K. Gabrielson, D.B. Rifkin, L. Carta, F. Ramirez, D.L. Huso, H.C. Dietz, Losartan, an AT1 antagonist, prevents aortic aneurysm in a mouse model of Marfan syndrome, Science 312 (5770) (2006) 117–121, https://doi.org/10.1126/science.1124287.
[15] T. Sato, M. Arakawa, Y. Tashima, E. Tsuboi, G. Burdon, J. Trojan, T. Koyano, Y. N. Youn, K. Penov, A.J. Pedroza, M. Shabazzi, I. Palmon, M.N. Nguyen, A. J. Connolly, A. Yamaguchi, M.P. Fischbein, Statins reduce thoracic aortic aneurysm growth in marfan syndrome mice via inhibition of the ras-induced ERK (extracellular signal-regulated kinase) signaling pathway, J. Am. Heart Assoc. 7 (21) (2018), e008543, https://doi.org/10.1161/JAHA.118.008543.
[16] J. Golledge, Abdominal aortic aneurysm: update on pathogenesis and medical treatments, Nat. Rev. Cardiol. 16 (4) (2019) 225–242, https://doi.org/10.1038/s41569-018-0114-9.
[17] L. Muino-Mosquera, J. De Backer, Angiotensin-II receptor blockade in Marfan syndrome, Lancet 394 (10216) (2019) 2206–2207, https://doi.org/10.1016/S0140-6736(19)32536-X.
[18] K. Yoshimura, A. Nagasawa, J. Kudo, M. Onoda, N. Morikage, A. Furutani, H. Aoki, K. Hamano, Inhibitory effect of statins on inflammation-related pathways in human abdominal aortic aneurysm tissue, Int. J. Mol. Sci. 16 (5) (2015) 11213–11228, https://doi.org/10.3390/ijms160511213.
[19] S. Liao, M. Miralles, B.J. Kelley, J.A. Curci, M. Borhani, R.W. Thompson, Suppression of experimental abdominal aortic aneurysms in the rat by treatment with angiotensin-converting enzyme inhibitors, J. Vasc. Surg. 33 (5) (2001) 1057–1064, https://doi.org/10.1067/mva.2001.112810.
[20] Q. Hao, X. Dong, X. Chen, F. Yan, X. Wang, H. Shi, B. Dong, Angiotensin-converting enzyme 2 inhibits angiotensin II-induced abdominal aortic aneurysms in mice, Hum. Gene Ther. 29 (12) (2018) 1387–1395, https://doi.org/10.1089/hum.2016.144.
[21] K. Yoshimura, N. Morikage, S. Nishino-Fujimoto, A. Furutani, B. Shirasawa, K. Hamano, Current status and perspectives on pharmacologic therapy for

abdominal aortic aneurysm, Curr. Drug Targets 19 (11) (2018) 1265–1275, https://doi.org/10.2174/1389450119666171227223331.
[22] Y. Xu, J. Peng, X. Dong, H. Li, J. Chang, Combined chemical and structural signals of biomaterials synergistically activate cell-cell communications for improving tissue regeneration, Acta Biomater. 55 (2017) 249–261, https://doi.org/10.1016/j.actbio.2017.03.056.
[23] L. Ma, Y. Zhou, Z. Zhang, Y. Liu, D. Zhai, H. Zhuang, Q. Li, J. Yuye, C. Wu, J. Chang, Multifunctional bioactive Nd-Ca-Si glasses for fluorescence thermometry, photothermal therapy, and burn tissue repair, Sci. Adv. 6 (32) (2020), https://doi.org/10.1126/sciadv.abb1311 eabb1311.
[24] Y. Huang, C. Wu, X. Zhang, J. Chang, K. Dai, Regulation of immune response by bioactive ions released from silicate bioceramics for bone regeneration, Acta Biomater. 66 (2018) 81–92, https://doi.org/10.1016/j.actbio.2017.08.044.
[25] H. Li, W. Wang, J. Chang, Calcium silicate enhances immunosuppressive function of MSCs to indirectly modulate the polarization of macrophages, Regen. Biomater. 8 (6) (2021), https://doi.org/10.1093/rb/rbab056 rbab056.
[26] I. Pineda-Torra, M. Gage, A. de Juan, O.M. Pello, Isolation, culture, and polarization of murine bone marrow-derived and peritoneal macrophages, Methods Mol. Biol. 1339 (2015) 101–109, https://doi.org/10.1007/978-1-4939-2929-0_6.
[27] Y. Que, X. Shu, L. Wang, S. Wang, S. Li, P. Hu, X. Tong, Inactivation of SERCA2 Cys (674) accelerates aortic aneurysms by suppressing PPARgamma, Br. J. Pharmacol. 178 (11) (2021) 2305–2323, https://doi.org/10.1111/bph.15411.
[28] Y.Y. Yang, L.Y. Li, X.L. Jiao, L.X. Jia, X.P. Zhang, Y.L. Wang, S. Yang, J. Li, J. Du, Y. X. Wei, Y.W. Qin, Intermittent hypoxia alleviates beta-aminopropionitrile monofumarate induced thoracic aortic dissection in C57BL/6 mice, Eur. J. Vasc. Endovasc. Surg. 59 (6) (2020) 1000–1010, https://doi.org/10.1016/j.ejvs.2019.10.014.
[29] A. Daugherty, M.W. Manning, L.A. Cassis, Angiotensin II promotes atherosclerotic lesions and aneurysms in apolipoprotein E-deficient mice, J. Clin. Invest. 105 (11) (2000) 1605–1612, https://doi.org/10.1172/JCI7818.
[30] G. Liu, F. Wu, X. Jiang, Y. Que, Z. Qin, P. Hu, K.S.S. Lee, J. Yang, C. Zeng, B. D. Hammock, X. Tong, Inactivation of Cys(674) in SERCA2 increases BP by inducing endoplasmic reticulum stress and soluble epoxide hydrolase, Br. J. Pharmacol. 177 (8) (2020) 1793–1805, https://doi.org/10.1111/bph.14937.
[31] W. Yu, S. Li, H. Wu, P. Hu, L. Chen, C. Zeng, X. Tong, Endothelial Nox4 dysfunction aggravates atherosclerosis by inducing endoplasmic reticulum stress and soluble epoxide hydrolase, Free Radic. Biol. Med. 164 (2021) 44–57, https://doi.org/10.1016/j.freeradbiomed.2020.12.450.
[32] X. Zuo, H. Zhang, T. Zhou, Y. Duan, H. Shou, S. Yu, C. Gao, Spheroids of endothelial cells and vascular smooth muscle cells promote cell migration in hyaluronic acid and fibrinogen composite hydrogels, Research (Wash D C) 2020 (2020), 8970480, https://doi.org/10.34133/2020/8970480.
[33] C. Dong, C. Yang, M.R. Younis, J. Zhang, G. He, X. Qiu, L.H. Fu, D.Y. Zhang, H. Wang, W. Hong, J. Lin, X. Wu, P. Huang, Bioactive NIR-II light-responsive shape memory composite based on cuprorivaite nanosheets for endometrial regeneration, Adv Sci (Weinh) 9 (12) (2022), e2102220, https://doi.org/10.1002/advs.202102220.
[34] Q. Xu, F. Jiang, G. Guo, E. Wang, M.R. Younis, Z. Zhang, F. Zhang, Z. Huan, C. Fan, C. Yang, Targeted hot ion therapy of infected wound by glycol chitosan and polydopamine grafted Cu-SiO2 nanoparticles, Nano Today 41 (2021), 101330.
[35] M. Yi, H. Li, X. Wang, J. Yan, L. Gao, Y. He, X. Zhong, Y. Cai, W. Feng, Z. Wen, C. Wu, C. Ou, J. Chang, M. Chen, Ion therapy: a novel strategy for acute myocardial infarction, Adv. Sci. 6 (1) (2019), 1801260, https://doi.org/10.1002/advs.201801260.
[36] X. Wang, L. Gao, Y. Han, M. Xing, C. Zhao, J. Peng, J. Chang, Silicon-enhanced adipogenesis and angiogenesis for vascularized adipose tissue engineering, Adv. Sci. 5 (11) (2018), 1800776, https://doi.org/10.1002/advs.201800776.
[37] G. Jia, A.R. Aroor, C. Jia, J.R. Sowers, Endothelial cell senescence in aging-related vascular dysfunction, Biochim. Biophys. Acta, Mol. Basis Dis. 1865 (7) (2019) 1802–1809, https://doi.org/10.1016/j.bbadis.2018.08.008.
[38] T. Aschacher, O. Salameh, F. Enzmann, B. Messner, M. Bergmann, Telomere biology and thoracic aortic aneurysm, Int. J. Mol. Sci. 19 (1) (2017) 1–16, https://doi.org/10.3390/ijms19010003.
[39] H.Z. Chen, F. Wang, P. Gao, J.F. Pei, Y. Liu, T.T. Xu, X. Tang, W.Y. Fu, J. Lu, Y. F. Yan, X.M. Wang, L. Han, Z.Q. Zhang, R. Zhang, M.H. Zou, D.P. Liu, Age-associated sirtuin 1 reduction in vascular smooth muscle links vascular senescence and inflammation to abdominal aortic aneurysm, Circ. Res. 119 (10) (2016) 1076–1088, https://doi.org/10.1161/CIRCRESAHA.116.308895.
[40] A. Mojiri, B.K. Walther, C. Jiang, G. Matrone, R. Holgate, Q. Xu, E. Morales, G. Wang, J. Gu, R. Wang, J.P. Cooke, Telomerase therapy reverses vascular senescence and extends lifespan in progeria mice, Eur. Heart J. 42 (42) (2021) 4352–4369, https://doi.org/10.1093/eurheartj/ehab547.
[41] L.F. Chen, Y. Mu, W.C. Greene, Acetylation of RelA at discrete sites regulates distinct nuclear functions of NF-kappaB, EMBO J. 21 (23) (2002) 6539–6548, https://doi.org/10.1093/emboj/cdf660.
[42] G. Lian, X. Li, L. Zhang, Y. Zhang, L. Sun, X. Zhang, H. Liu, Y. Pang, W. Kong, T. Zhang, X. Wang, C. Jiang, Macrophage metabolic reprogramming aggravates aortic dissection through the HIF1alpha-ADAM17 pathway, EBioMedicine 49 (2019) 291–304, https://doi.org/10.1016/j.ebiom.2019.09.041.
[43] F. Andreata, V. Syvannarath, M. Clement, S. Delbosc, K. Guedj, G. Fornasa, J. Khallou-Laschet, M. Morvan, G. Even, E. Procopio, A.T. Gaston, M. Le Borgne, L. Deschamps, A. Nicoletti, G. Caligiuri, Macrophage CD31 signaling in dissecting aortic aneurysm, J. Am. Coll. Cardiol. 72 (1) (2018) 45–57, https://doi.org/10.1016/j.jacc.2018.04.047.
[44] M.A. Dale, M.K. Ruhlman, B.T. Baxter, Inflammatory cell phenotypes in AAAs: their role and potential as targets for therapy, Arterioscler. Thromb. Vasc. Biol. 35 (8) (2015) 1746–1755, https://doi.org/10.1161/ATVBAHA.115.305269.
[45] R. He, D.C. Guo, A.L. Estrera, H.J. Safi, T.T. Huynh, Z. Yin, S.N. Cao, J. Lin, T. Kurian, L.M. Buja, Y.J. Geng, D.M. Milewicz, Characterization of the inflammatory and apoptotic cells in the aortas of patients with ascending thoracic aortic aneurysms and dissections, J. Thorac. Cardiovasc. Surg. 131 (3) (2006) 671–678, https://doi.org/10.1016/j.jtcvs.2005.09.018.
[46] H.Y. Lu, C.M. Shih, C.Y. Huang, A.T.H. Wu, T.M. Cheng, F.L. Mi, C.C. Shih, Galectin-3 modulates macrophage activation and contributes smooth muscle cells apoptosis in abdominal aortic aneurysm pathogenesis, Int. J. Mol. Sci. 21 (21) (2020), https://doi.org/10.3390/ijms21218257.
[47] B. Zhou, W. Li, G. Zhao, B. Yu, B. Ma, Z. Liu, N. Xie, Y. Fu, Z. Gong, R. Dai, X. Zhang, W. Kong, Rapamycin prevents thoracic aortic aneurysm and dissection in mice, J. Vasc. Surg. 69 (3) (2019) 921–932, https://doi.org/10.1016/j.jvs.2018.05.246, e3.
[48] G. Katsuumi, I. Shimizu, Y. Yoshida, T. Minamino, Vascular senescence in cardiovascular and metabolic diseases, Front. Cardiovasc. Med. 5 (2018) 18, https://doi.org/10.3389/fcvm.2018.00018.
[49] C. Pisano, C.R. Balistreri, A. Ricasoli, G. Ruvolo, Cardiovascular disease in ageing: an overview on thoracic aortic aneurysm as an emerging inflammatory disease, Mediat. Inflamm. 2017 (2017), 1274034, https://doi.org/10.1155/2017/1274034.
[50] J.J. Boyle, P.L. Weissberg, M.R. Bennett, Tumor necrosis factor-alpha promotes macrophage-induced vascular smooth muscle cell apoptosis by direct and autocrine mechanisms, Arterioscler. Thromb. Vasc. Biol. 23 (9) (2003) 1553–1558, https://doi.org/10.1161/01.ATV.0000086961.44581.B7.
[51] A. Ghosh, L.V. Pechota, G.R. Upchurch Jr., J.L. Eliason, Cross-talk between macrophages, smooth muscle cells, and endothelial cells in response to cigarette smoke: the effects on MMP2 and 9, Mol. Cell. Biochem. 410 (1–2) (2015) 75–84, https://doi.org/10.1007/s11010-015-2539-3.
[52] G. Zhao, H. Lu, Z. Chang, Y. Zhao, T. Zhu, L. Chang, Y. Guo, M.T. Garcia-Barrio, Y. E. Chen, J. Zhang, Single-cell RNA sequencing reveals the cellular heterogeneity of aneurysmal infrarenal abdominal aorta, Cardiovasc. Res. 117 (5) (2021) 1402–1416, https://doi.org/10.1093/cvr/cvaa214.
[53] L. Sheng, Z. Zhang, Y. Zhang, E. Wang, B. Ma, Q. Xu, L. Ma, M. Zhang, G. Pei, J. Chang, A novel "hot spring"-mimetic hydrogel with excellent angiogenic properties for chronic wound healing, Biomaterials 264 (2021), 120414, https://doi.org/10.1016/j.biomaterials.2020.120414.
[54] X. Wang, L. Wang, Q. Wu, F. Bao, H. Yang, X. Qiu, J. Chang, Chitosan/calcium silicate cardiac patch stimulates cardiomyocyte activity and myocardial performance after infarction by synergistic effect of bioactive ions and aligned nanostructure, ACS Appl. Mater. Interfaces 11 (1) (2019) 1449–1468, https://doi.org/10.1021/acsami.8b17754.
[55] P. Zhou, D. Xia, Z. Ni, T. Ou, Y. Wang, H. Zhang, L. Mao, K. Lin, S. Xu, J. Liu, Calcium silicate bioactive ceramics induce osteogenesis through oncostatin M, Bioact. Mater. 6 (3) (2021) 810–822, https://doi.org/10.1016/j.bioactmat.2020.09.018.
[56] C. Yang, H. Ma, Z. Wang, M.R. Younis, C. Liu, C. Wu, Y. Luo, P. Huang, 3D printed wesselsite nanosheets functionalized scaffold facilitates NIR-II photothermal therapy and vascularized bone regeneration, Adv. Sci. 8 (20) (2021), e2100894, https://doi.org/10.1002/advs.202100894.
[57] T. Chen, Z. Zhang, D. Weng, L. Lu, X. Wang, M. Xing, H. Qiu, M. Zhao, L. Shen, Y. Zhou, J. Chang, H.P. Li, Ion therapy of pulmonary fibrosis by inhalation of ionic solution derived from silicate bioceramics, Bioact. Mater. 6 (10) (2021) 3194–3206, https://doi.org/10.1016/j.bioactmat.2021.02.013.
[58] X. Dong, J. Chang, H. Li, Bioglass promotes wound healing through modulating the paracrine effects between macrophages and repairing cells, J. Mater. Chem. B. 5 (26) (2017) 5240–5250, https://doi.org/10.1039/c7tb01211j.
[59] B. Buffoli, E. Foglio, E. Borsani, C. Exley, R. Rezzani, L.F. Rodella, Silicic acid in drinking water prevents age-related alterations in the endothelium-dependent vascular relaxation modulating eNOS and AQP1 expression in experimental mice: an immunohistochemical study, Acta Histochem. 115 (5) (2013) 418–424, https://doi.org/10.1016/j.acthis.2012.10.002.
[60] S. Villahoz, P.S. Yunes-Leites, N. Mendez-Barbero, K. Urso, E. Bonzon-Kulichenko, S. Ortega, J.F. Nistal, J. Vazquez, S. Offermanns, J.M. Redondo, M.R. Campanero, Conditional deletion of Rcan1 predisposes to hypertension-mediated intramural hematoma and subsequent aneurysm and aortic rupture, Nat. Commun. 9 (1) (2018) 4795, https://doi.org/10.1038/s41467-018-07071-7.
[61] C.L. Lino Cardenas, C.W. Kessinger, Y. Cheng, C. MacDonald, T. MacGillivray, B. Ghoshhajra, L. Huleihel, S. Nuri, A.S. Yeri, F.A. Jaffer, N. Kaminski, P. Ellinor, N. L. Weintraub, R. Malhotra, E.M. Isselbacher, M.E. Lindsay, An HDAC9-MALAT1-BRG1 complex mediates smooth muscle dysfunction in thoracic aortic aneurysm, Nat. Commun. 9 (1) (2018) 1009, https://doi.org/10.1038/s41467-018-03394-7.
[62] R.M. Touyz, R. Alves-Lopes, F.J. Rios, L.L. Camargo, A. Anagnostopoulou, A. Arner, A.C. Montezano, Vascular smooth muscle contraction in hypertension, Cardiovasc. Res. 114 (4) (2018) 529–539, https://doi.org/10.1093/cvr/cvy023.
[63] H. Lu, J. Sun, W. Liang, Z. Chang, O. Rom, Y. Zhao, G. Zhao, W. Xiong, H. Wang, T. Zhu, Y. Guo, L. Chang, M.T. Garcia-Barrio, J. Zhang, Y.E. Chen, Y. Fan, Cyclodextrin prevents abdominal aortic aneurysm via activation of vascular smooth muscle cell transcription factor EB, Circulation 142 (5) (2020) 483–498, https://doi.org/10.1161/CIRCULATIONAHA.119.044803.
[64] T. Hadi, L. Boytard, M. Silvestro, D. Alebrahim, S. Jacob, J. Feinstein, K. Barone, W. Spiro, S. Hutchison, R. Simon, D. Rateri, F. Pinet, D. Fenyo, M. Adelman, K. J. Moore, H.K. Eltzschig, A. Daugherty, B. Ramkhelawon, Macrophage-derived netrin-1 promotes abdominal aortic aneurysm formation by activating MMP3 in

vascular smooth muscle cells, Nat. Commun. 9 (1) (2018) 5022, https://doi.org/10.1038/s41467-018-07495-1.

[65] T. Saito, Y. Hasegawa, Y. Ishigaki, T. Yamada, J. Gao, J. Imai, K. Uno, K. Kaneko, T. Ogihara, T. Shimosawa, T. Asano, T. Fujita, Y. Oka, H. Katagiri, Importance of endothelial NF-kappaB signalling in vascular remodelling and aortic aneurysm formation, Cardiovasc. Res. 97 (1) (2013) 106–114, https://doi.org/10.1093/cvr/cvs298.

[66] C. Liu, C. Zhang, L. Jia, B. Chen, L. Liu, J. Sun, W. Zhang, B. You, Y. Li, P. Li, J. Du, Interleukin-3 stimulates matrix metalloproteinase 12 production from macrophages promoting thoracic aortic aneurysm/dissection, Clin. Sci. 132 (6) (2018) 655–668, https://doi.org/10.1042/CS20171529.

[67] E. van der Meij, G.G. Koning, P.W. Vriens, M.F. Peeters, C.A. Meijer, K. E. Kortekaas, R.L. Dalman, J.H. van Bockel, R. Hanemaaijer, T. Kooistra, R. Kleemann, J.H. Lindeman, A clinical evaluation of statin pleiotropy: statins selectively and dose-dependently reduce vascular inflammation, PLoS One 8 (1) (2013), e53882, https://doi.org/10.1371/journal.pone.0053882.